Tumour ischemia by Interferon-γ resembles physiological blood vessel regression

Thomas Kammertoens[1,2], Christian Friese[1,2], Ainhoa Arina[3], Christian Idel[4*], Dana Briesemeister[1,2], Michael Rothe[1,2], Andranik Ivanov[5], Anna Szymborska[2], Giannino Patone[2], Severine Kunz[2], Daniel Sommermeyer[2], Boris Engels[2], Matthias Leisegang[1,2,5], Ana Textor[1,2], Hans Joerg Fehling[6], Marcus Fruttiger[7], Michael Lohoff[8], Andreas Herrmann[9], Hua Yu[9], Ralph Weichselbaum[3], Wolfgang Uckert[2,5], Norbert Hübner[2,10,11], Holger Gerhardt[2,5,11], Dieter Beule[5], Hans Schreiber[1,4,5], and Thomas Blankenstein[1,2,5]

[1]Institute of Immunology, Charité Campus Buch, Berlin, Germany
[2]Max-Delbrück-Center for Molecular Medicine, Berlin, Germany
[3]Department of Radiation and Cellular Oncology, The University of Chicago, Chicago, USA
[4]Department of Pathology, The University of Chicago, Chicago, USA
[5]Berlin Institute of Health, Berlin, Germany
[6]Institute of Immunology, University Clinics Ulm, Ulm, Germany
[7]Institute of Ophthalmology, University College London, London, United Kingdom
[8]Institute for Medical Microbiology, University of Marburg, Marburg, Germany
[9]Beckman Research Institute at the Comprehensive Cancer Center City of Hope, Los Angeles, USA
[10]Charité-Universitätsmedizin, Berlin, Germany
[11]DZHK (German Center for Cardiovascular Research), partner site Berlin, Berlin, Germany
[*]Current address: Department for Otorhinolaryngology, University of Luebeck, Luebeck, Germany

Correspondence should be addressed to Thomas Blankenstein [tblanke@mdc-berlin.de]

Keywords: IFNγ, endothelial cell, ischemia, tumour necrosis

The relative contribution of T-cell produced effector molecules to tumour rejection is unclear, but interferon-γ (IFNγ) is critical in most models analysed[1]. While IFNγ can impede tumour growth by directly acting on the cancer cells[2,3], it has to act on the tumour stroma for rejection of large established tumours[4,5]. However, which stroma cells have to respond to IFNγ and by which mechanism IFNγ contributes to tumour rejection through stromal targeting remained elusive. Here, we used a model of IFNγ and IFNγ-GFP fusion protein induction in large vascularized tumours, growing in mice expressing the IFNγ receptor exclusively in defined cell types. Neither responsiveness to IFNγ by myeloid cells, other hematopoietic cells including T cells or fibroblasts was sufficient for IFNγ-induced tumour regression, while responsiveness to IFNγ by endothelial cells was necessary and sufficient. Intra-vital microscopy revealed IFNγ-induced regression of the tumour vasculature, resulting in blood flow arrest and subsequent tumour collapse, similar to non-haemorrhagic necrosis in ischemia but unlike haemorrhagic necrosis induced by tumour necrosis factor (TNF). The early events of IFNγ-induced tumour ischemia resemble non-apoptotic blood vessel regression during development, wound healing or IFNγ-mediated, pregnancy-induced remodelling of uterine arteries[6-8].

The contribution of T-cell effector molecules to tumour rejection has mainly been studied in models of low tumour burden with little tumour stroma[1,9]. For IFNγ-mediated effects, various cell types have been suggested as targets, such as the cancer cells themselves, macrophages, fibroblasts, monocytes or endothelial cells[10-18]. Most cells express the IFNγ receptor (IFNγR). IFNγ inhibits neo-angiogenesis and prevents the development of tumours from inoculated cancer cells[12,13], but which effect IFNγ has on the blood vessels of large established tumours is poorly understood. Since human cancers are usually at least one centimetre in diameter when first detected, studying the effects of IFNγ on the vasculature of such tumours is clinically relevant. We transduced the fibrosarcoma cell line MCA313, derived from a methylcholanthrene-treated IFNγR-deficient C57BL/6 ($IFN\gamma R^{del}$) mouse, with a retrovirus allowing doxycycline (dox)-mediated regulation of IFNγ expression ($MCA313^{IFN\gamma\text{-}IND}$)[19,20] (Fig. 1a). $MCA313^{IFN\gamma\text{-}IND}$ cells produced IFNγ upon dox treatment (~87 ng/ml), but not in its absence (Fig. 1b). When IFNγ was induced in large $MCA313^{IFN\gamma\text{-}IND}$ tumours in Rag-deficient (Rag^{del}) mice, serum levels reached a peak of ~10 ng/ml 48 h after dox administration (Fig. 1c). Induction of IFNγ in 3 weeks-old large $MCA313^{IFN\gamma\text{-}IND}$ tumours in C57BL/6 wild type

(WT) mice led to tumour regression, macroscopic as well as microscopic necrosis and loss of tumour endothelial ($CD31^+$) cells (Extended Data Fig. 1a-c). Tumour regression was observed in WT but not in $IFN\gamma R^{del}$ mice (Extended Data Fig. 1a). $MCA313^{IFN\gamma\text{-}IND}$ tumours grew with similar kinetics and regressed similarly upon IFNγ induction in WT and Rag^{del} mice, indicating their low immunogenicity (Extended Data Fig. 1a). To determine whether dox-induced IFNγ levels were comparable to those achieved by antigen-specific T cells rejecting established tumours of a similar size, we treated Rag^{del} mice bearing 16.113 tumours with TCR-I $CD8^+$ T cells specific for SV40 Large T antigen expressed by the cancer cells and determined IFNγ serum levels 3-7 days after T-cell transfer. On day 4, ~13 ng/ml IFNγ were detected (Fig. 1c) and tumours were subsequently rejected (Extended Data Fig. 1d). Thus, IFNγ expression in large $MCA313^{IFN\gamma\text{-}IND}$ tumours was comparable to that of effector T cells during tumour rejection and was sufficient to induce tumour regression, if only tumour stroma but not cancer cells could respond to IFNγ. Similarly, IFNγ induction in large IFNγ-insensitive $16.113\text{-}999^{IFN\gamma\text{-}IND}$ adenocarcinomas resulted in tumour regression and a reduction in tumour endothelial cells (Extended Data Fig. 1e-g).

To identify the stromal target cells of IFNγ, we generated mice with exclusive IFNγR expression in defined cell types. In these mice, the IFNγR transgene is linked to a GFP reporter gene by an internal ribosome entry site (IRES) and separated from a ubiquitous promoter by a Cre recombinase-excisable stop cassette ($pCAG^{loxP}Stop^{loxP}$-IFNγR-IRES-GFP, termed PIG mice, Fig. 1a and Extended Data Fig. 2a). The mice were crossed to $IFN\gamma R^{del}$ mice to inactivate their endogenous IFNγR gene ($PIG^{IFN\gamma R\text{-}del}$). Expression of the Cre recombinase in fibroblasts from $PIG^{IFN\gamma R\text{-}del}$ mice led to IFNγR (CD119) and GFP expression (Extended Data Fig. 2b). IFNγ up-regulated MHC-I comparable to WT fibroblasts, demonstrating function and tight regulation of the IFNγR (Extended Data Fig. 2c). We generated $PIG^{IFN\gamma R\text{-}del}$ x CMV-Cre ($PIG^{Cmv\text{-}Cre}$) mice with ubiquitous Cre recombinase expression. Most stroma cells of $MCA313^{IFN\gamma\text{-}IND}$ tumours grown in $PIG^{Cmv\text{-}Cre}$ mice were GFP^+, as analysed for $CD11b^+$ (myeloid), $F4/80^+$ (macrophages), $CD31^+$ (endothelial), and FAP^+ (mesenchymal) cells (Extended Data Fig. 2d). Most cells in the peripheral blood (T cells, B cells, NK cells, $CD11b^+$, $CD11c^+$, $GR1^+$ cells) were GFP^+ (Supplementary Data Table 1a). No GFP^+ cells were detected in $MCA313^{IFN\gamma\text{-}IND}$ tumours of $PIG^{IFN\gamma R\text{-}del}$ mice (Supplementary Data Table 1b and Extended Data Fig. 2e). Dox-induced IFNγ expression in large $MCA313^{IFN\gamma\text{-}IND}$ tumours in $PIG^{Cmv\text{-}Cre}$ but not in $PIG^{IFN\gamma R\text{-}del}$ mice induced necrosis, loss of endothelial cells and tumour regression, indicating that the model allowed the identification of the stromal targets of IFNγ (Fig. 1d-i).

Since ($Tie2^+$) macrophages support neo-vascularization in tumours[21] but can also secrete anti-angiogenic cytokines in response to IFNγ[14,15], we analysed $PIG^{IFNγR\text{-}del}$ x Lys-Cre ($PIG^{Lys\text{-}Cre}$) mice with exclusive IFNγR expression in cells of the myeloid lineage (Supplementary Data Table 1a). In $MCA313^{IFNγ\text{-}IND}$ tumours, most $CD11b^+$ and $F4/80^+$ cells, but not $CD31^+$ or FAP^+ cells, were GFP^+ and, thus, IFNγ-responsive (Extended Data Fig. 3a). IFNγ induction in established $MCA313^{IFNγ\text{-}IND}$ tumours of $PIG^{Lys\text{-}Cre}$ mice neither induced necrosis, nor reduced numbers of endothelial ($CD31^+$) cells, nor delayed tumour growth (Fig. 2a-c). Thus, exposing exclusively myeloid cells in established tumours to IFNγ does not lead to cancer regression.

We generated $PIG^{IFNγR\text{-}del}$ x FSP-Cre ($PIG^{Fsp\text{-}Cre}$) mice in which one fourth of tail fibroblasts and most haematopoietic cells but not endothelial cells expressed GFP and, thus, the IFNγR (Extended Data Fig. 3b and Supplementary Data Table 1a). In $MCA313^{IFNγ\text{-}IND}$ tumours, $CD11b^+$, $F4/80^+$ and FAP^+ cells, but not $CD31^+$ cells had recombined, as indicated by GFP expression (Extended Data Fig. 3c). IFNγ induction in established $MCA313^{IFNγ\text{-}IND}$ tumours of $PIG^{Fsp\text{-}Cre}$ mice did not lead to macroscopic necrosis, microscopic endothelial cell loss or tumour regression (Fig. 2d-f). To confirm that IFNγ-signalling in T cells does not contribute to blood vessel reduction, we reconstituted Rag^{del} or Rag^{del} x $IFNγR^{del}$ mice with WT splenocytes and induced IFNγ in established $MCA313^{IFNγ\text{-}IND}$ tumours. Only in T cell-reconstituted Rag^{del} but not Rag^{del} x $IFNγR^{del}$ recipients endothelial cell numbers were reduced after IFNγ induction (Extended Data Fig. 3d). Thus, IFNγ responsiveness by tumour-associated fibroblasts, T cells or hematopoietic cells was not sufficient for IFNγ-induced tumour necrosis or regression.

Next, we analysed mice with selective IFNγR expression in endothelial cells using PDGFB-CreER-IRES-GFP mice. Because these mice, in which recombination is tamoxifen-inducible in $PDGFB^+$ cells, and $PIG^{IFNγR\text{-}del}$ mice both carry GFP reporter genes, recombination was analysed in tamoxifen-treated PDGFB-CreER-IRES-GFP x Rosa26-RFP mice bearing large $MCA313^{IFNγ\text{-}IND}$ tumours. Around 75.4% of tumour endothelial cells ($CD31^+/CD146^+$) had recombined, indicated by RFP expression (Extended Data Fig. 4a, b). To avoid confounding effects by endogenous IFNγ (Extended Data Fig. 4c-g), experiments were performed in quadruple $PIG^{IFNγR\text{-}del}$ x PDGFB-CreER-IRES-GFP x $IFNγ^{del}$ ($PIG^{Pdgfb\text{-}Cre\text{-}IFNγ\text{-}del}$) transgenic mice, which are deficient in IFNγ and IFNγR expression and allow selective induction of IFNγR expression in endothelial cells. GFP was almost exclusively expressed in tumour endothelial cells and faithfully monitored IFNγR expression (Extended Data Fig. 5a, b). The few GFP^+ $CD11b^+$ cells did not respond to IFNγ with INOS induction

(Supplementary Data Table 1b and Extended Data Fig. 5c). IFNγ induction in large MCA313$^{IFNγ\text{-}IND}$ tumours in tamoxifen-treated PIG$^{Pdgfb\text{-}Cre\text{-}IFNγ\text{-}del}$ mice induced necrosis, disappearance of endothelial cells and tumour regression (Fig. 2g-i). Following regression, tumours slowly resumed growth (Fig. 2i). However, these tumours contained large central necrotic areas with viable cells at the rim (Extended Data Fig. 5d, e). As opposed to endothelial cells without IFNγ induction, endothelial cells in tumours exposed for ~ 50 days to IFNγ were mostly GFP$^-$, suggesting a strong selective pressure against IFNγR-expressing endothelial cells (Fig. 2j). In line with this assumption, tumours grown for 50-100 days in PIG$^{Pdgfb\text{-}Cre}$ or PIG$^{Cmv\text{-}Cre}$ mice still produced inducible IFNγ in vitro (Extended Data Figure 5f). After five days of IFNγ exposure, endothelial cells (CD31$^+$/CD146$^+$) in MCA313$^{IFNγ\text{-}IND}$ tumours of all mice investigated in this study were reduced by 80-90% only in those lines, in which endothelial cells could respond to IFNγ (Fig. 2k). To ask whether T cell-derived IFNγ similarly affects endothelial cells, Rag^{del} mice bearing 16.113 tumours were treated with IFNγ-competent or -deficient TCR-I CD8$^+$ T cells. Five days after T cell transfer, we found a significantly lower number of endothelial cells in tumours treated with WT than with IFNγ-deficient T cells (Extended Data Fig. 1h). Together, IFNγR responsiveness by tumour endothelial cells was necessary and sufficient for necrosis and tumour regression.

We intravitally imaged the same area of tumours that were growing behind a glass window over several days[22]. To better assess the kinetics of vascular regression by IFNγ, a dox-inducible IFNγ-GFP fusion gene was introduced into plasmacytoma J558L cells (J558L$^{IFNγ\text{-}GFP\text{-}IND}$), which are resistant to cytotoxic effects of IFNγ and TNF (see below)[23]. To monitor cancer cells, J558L$^{IFNγ\text{-}GFP\text{-}IND}$ cells additionally expressed the fluorescent (cerulean) protein. J558L$^{IFNγ\text{-}GFP\text{-}IND}$ cells produced ~104 ng/ml biologically active IFNγ-GFP (Fig. 3a, b) and could be visualized by intravital microscopy (Supplementary Information Video 1 and 2). Its induction in established J558L$^{IFNγ\text{-}GFP\text{-}IND}$ tumours growing in Rag^{del} mice led to tumour regression (Extended Data Fig. 6a). Large vascularized J558L$^{IFNγ\text{-}GFP\text{-}IND}$ tumours growing behind a window were imaged for 6 days following dox application. A GFP signal was observed 24 h after IFNγ-GFP induction, and vascular density decreased with a loss of smaller blood vessels and thinning of larger vessels (Fig. 3c). At 48 h, blood vessels further decreased and were undetectable by 96 h of dox treatment. As shown by loss of cerulean signal, cancer cells were destroyed subsequent to blood vessel regression (Fig. 3d and Extended Data Fig. 6b). DiD-labelled erythrocytes, injected before imaging, did not leak from the tumour vessels during the entire longitudinal imaging. Instead, the blood flow ceased with

progressing vessel regression (Supplementary Information Video 3). Thus, IFNγ induced tumour ischemia.

We performed similar experiments with TNF, which is usually produced simultaneously with IFNγ by activated T cells. Therefore, cerulean^{+} J558L$^{\text{TNF-GFP-IND}}$ cells with an inducible TNF-GFP fusion protein were generated. J558L$^{\text{TNF-GFP-IND}}$ produced ~368 pg/ml biologically active TNF-GFP upon dox application (Fig. 3e, f). Induction of TNF-GFP in established J558L$^{\text{TNF-GFP-IND}}$ tumours growing in Rag$^{\text{del}}$ mice led to tumour regression (Extended Data Fig. 7a). Imaging revealed strikingly different changes caused by TNF-GFP compared to IFNγ-GFP. The TNF-GFP signal was observed after 24 h. Blood vessels did not become thinner but, if anything, wider (Fig. 3g and Extended Data Fig. 7b). By ~36 h after TNF-GFP induction, the blood vessels burst and DiD-labelled erythrocytes leaked into the tumour tissue (Supplementary Information Video 4). Cancer cells decayed subsequent to vessel burst (Fig. 3h). In J558L$^{\text{TNF-GFP-IND}}$ tumours, erythrocytes were dispersed throughout the tissue 48 h after TNF-GFP induction, whereas in J558L$^{\text{IFNγ-GFP-IND}}$ tumours they remained within blood vessels (Extended Data Fig. 8a, b). Together, necrosis caused by IFNγ was induced by ischemic shutdown of perfusion rather than by bursting of the blood vessels as observed for TNF.

Endothelial cells in kidney and spleen of WT mice 5 days after dox treatment were unaltered (Extended Data Fig. 9a), indicating a relative selective effect on the (activated) tumour vasculature. Gene expression profiling of normal kidney and tumour endothelial cells revealed 1500 differentially expressed genes. After IFNγ induction, the expression of 356 genes changed in kidney and 42 in tumour endothelial cells. Only 17 genes were exclusively regulated in tumour endothelial cells (Extended Data Fig. 9b). Activated endothelium occurs physiologically, e.g. during development, pregnancy-induced vascular remodelling and wound healing. In PIG$^{\text{Pdgfb-Cre-IFNγ-del}}$ mice and WT mice with elevated IFNγ levels from small MCA313$^{\text{IFNγ-IND}}$ tumours, wounds did not heal in contrast to IFNγR$^{\text{del}}$ mice, suggesting a selective effect of IFNγ on activated endothelium (Extended Data Fig. 5 g, h). To further elaborate on this hypothesis, we determined the gene expression profile of IFNγ-exposed endothelial cells of MCA313$^{\text{IFNγ-IND}}$ and J558L$^{\text{IFNγ-GFP-IND}}$ tumours as well as 16.113 tumours treated by adoptive T cell therapy (Extended Data Fig. 9c and Supplementary Table 2). Endothelial cells from all three tumours showed strong similarity in regulated genes. Genes associated with immune regulation and migration, e.g. CXCL10 and CXCL11 (Extended Data Fig. 9c and Supplementary Data Table 2) were highly regulated. It is well-established that CXCL10 acts anti-angiogenic on tumour blood vessels and is involved in physiological vessel

regression, but it was surprising that it is produced by the tumour endothelial cells themselves[7,14-16].

We did not observe apoptosis-associated genes to be highly regulated in IFNγ-exposed endothelial cells (Supplementary Table 2). Rather, IFNγ-exposed endothelial (ERG^+ or $CD31^+$) cells in $MCA313^{IFN\gamma\text{-}IND}$ tumours gradually decreased over a five-days period (Extended Data Fig. 10a-e). Even though the total cleaved caspase 3^+ ($CC3^+$) area increased (Extended Data Fig. 10f), the number of $CC3^+$ endothelial cells did not (Extended Data Fig. 10c). Endothelial cells significantly decreased not only in necrotic but also in vital tumour tissue (Extended Data Fig. 10b). Reduction in endothelial cells preceded decrease in collagen 4 (Extended Data Fig. 10g-i). $NG2^+$ pericytes did not decrease (Extended Data Fig. 10j, k), and we did not observe reduced co-localization with endothelial cells (Extended Data Fig. 10l). Therefore, we assume that primarily pericyte-uncovered endothelial cells disappeared during the first five days of IFNγ exposure. IFNγ exposure led to rapid rounding and condensation of $CD31^+$ and VE-cadherin$^+$ endothelial cells in $MCA313^{IFN\gamma\text{-}IND}$ tumours, similar as observed for regressing blood vessels during the ovarian cycle (Extended Data Fig. 10m)[24,25]. In line with earlier studies on physiological blood vessel regression[25], electron microscopy showed that the vessels were more frequently occluded upon IFNγ exposure (Extended Data Figure 10n, o). IFNγ induced also profound morphological changes of human umbilical vein endothelial cells in vitro without indication of apoptosis (Extended Data Fig. 9e and Supplementary Information Video 5). In the J558L model, we confirmed reduction of endothelial (ERG^+ or $CD31^+$) cells by IFNγ-GFP fusion protein (Extended Data Fig. 6c-g) and found that TNF-GFP did not significantly change endothelial cell numbers during the first five days of cytokine exposure (Extended Data Fig. 7f, g). Collectively, we observed a process, which involves lumen collapse/vessel occlusion and progressive disappearance of first small and then large calibre vessels. These characteristics of controlled blood vessel regression suggest that IFNγ induces changes in the tumour vasculature similar to those observed during physiological blood vessel regression. *Irf4*, up-regulated by IFNγ in tumour but not normal endothelial cells (Extended Data Fig. 9b, c, Supplementary Table 2), has not been reported to be induced by IFNγ in (tumour-) endothelial cells. It was induced in vitro by IFNγ in mouse endothelial cells (Extended Data Fig. 9f). Endothelial cells in large $MCA313^{IFN\gamma\text{-}IND}$ tumours two days after IFNγ induction in *Irf4*-deficient mice revealed a more pronounced vessel reduction (Extended Data Figure 9g, h) and an increased number of apoptotic endothelial cells compared to those in WT mice (Extended Data Fig. 9i, j), reminiscent to the protective role of IRF4 for neurons in ischemia[26].

We showed that ischemia, a pathological reaction, is beneficial in anti-tumour responses. Both, IFNγ and TNF destroy tumour blood vessels, yet by different mechanisms and with different consequences. IFNγ released by the tumour did not lead to systemic toxicity in mice with selective IFNγR expression on endothelial cells, as observed in WT mice, which is compatible with the observation that IFNγ, unlike TNF, does not induce necrosis in combination with bacterial products in the normal skin[27]. The early events induced by IFNγ in tumours resemble blood vessel regression in development, wound healing, ovary cycle and pregnancy-induced uterine vascular remodelling, the latter being regulated by IFNγ[6-8,24,25]. In conclusion, IFNγ and TNF, simultaneously produced by effector T cells, are a powerful team: 1. TNF bursts the tumour vessels and allows extravasation of infiltrating cells, and 2. IFNγ helps to prevent relapse by keeping the tumour in an ischemic state, similar as observed when targeting these cytokines selectively to the vasculature[28].

References

1. Blankenstein, T. The role of tumor stroma in the interaction between tumor and immune system. *Curr. Opin. Immunol.* **17**, 180-186 (2005).

2. Dighe, A.S., Richards, E., Old, L. J. & Schreiber, R. D. Enhanced in vivo growth and resistance to rejection of tumor cells expressing dominant negative IFN gamma receptors. *Immunity* **1**, 447-456 (1994).

3. Braumuller, H. *et al*. T-helper-1-cell cytokines drive cancer into senescence. *Nature* **494**, 361-365 (2013).

4. Zhang, B., Karrison, T., Rowley, D. A. & Schreiber, H. IFN-gamma- and TNF-dependent bystander eradication of antigen-loss variants in established mouse cancers. *J. Clin. Invest.* **118**, 1398-1404 (2008).

5. Listopad, J. J. *et al*. Fas expression by tumor stroma is required for cancer eradication. *Proc. Natl. Acad. Sci. USA* **110**, 2276-2281 (2013).

6. Franco C.A. *et al*. Dynamic endothelial cell rearrangements drive developmental vessel regression. *PLoS Biol*. e1002125 (2015).

7. Bodnar, R. J. *et al*. IP-10 induces dissociation of newly formed blood vessels. *J. Cell Sci*. **122**, 2064-2077 (2009).

8. Ashkar A.A., Di Santo J.P. & Croy B.A. Interferon gamma contributes to initiation of uterine vascular modification, decidual integrity, and uterine natural killer cell maturation during normal murine pregnancy. *J. Exp. Med.* **192**, 259-70 (2000).

9. Schreiber, K., Rowley, D. A., Riethmuller, G. & Schreiber, H. Cancer immunotherapy and preclinical studies: why we are not wasting our time with animal experiments. *Hematol. Oncol. Clinics North Am.* **20**, 567-584 (2006).

10. Corthay, A. *et al*. Primary antitumor immune response mediated by CD4+ T cells. *Immunity* **22**, 371-383 (2005).

11. Lu *et al*. Responsiveness of stromal fibroblasts to IFN-gamma blocks tumor growth via angiostasis. *J. Immunol.* **183**, 6413-6421 (2009).

12. Qin Z. & Blankenstein T. $CD4^+$ T cell-mediated tumor rejection involves inhibition of angiogenesis that is dependent on IFN-γ receptor expression by nonhematopoietic cells. *Immunity* **12**, 677-686 (2000).

13. Qin, Z. *et al*. A critical requirement of interferon gamma-mediated angiostasis for tumor rejection by $CD8^+$ T cells. *Cancer Res.* **63**, 4095-4100 (2003).

14. Coughlin, C. M. *et al*. Tumor cell responses to IFNgamma affect tumorigenicity and response to IL-12 therapy and antiangiogenesis. *Immunity* **9**, 25-34 (1998).

15. Luster, A. D., Unkeless, J. C. & Ravetch, J. V. Gamma-interferon transcriptionally regulates an early-response gene containing homology to platelet proteins. *Nature* **315**, 672-676 (1985).

16. Sgadari, C. *et al*. Mig, the monokine induced by interferon-gamma, promotes tumor necrosis in vivo. *Blood* **89**, 2635-2643 (1997).

17. Deng, J. *et al*. IFNγ-responsiveness of endothelial cells leads to efficient angiostasis in tumours involving down-regulation of Dll4. *J. Pathol*. **233**, 170-182 (2014).

18. Tellides, G. *et al*. Interferon-gamma elicits arteriosclerosis in the absence of leukocytes. *Nature* **403**, 207-211 (2000).

19. Briesemeister, D. *et al*. Tumor rejection by local interferon gamma induction in established tumors is associated with blood vessel destruction and necrosis. *Int. J. Cancer* **128**, 371-378 (2011).

20. Anders, K. *et al*. Oncogene-targeting T cells reject large tumors while oncogene inactivation selects escape variants in mouse models of cancer. *Cancer Cell* **20**, 755-767 (2011).

21. Mazzieri, R. *et al*. Targeting the ANG2/TIE2 axis inhibits tumor growth and metastasis by impairing angiogenesis and disabling rebounds of proangiogenic myeloid cells. *Cancer Cell* **19**, 512-526 (2011).

22. Schietinger, A. *et al*. Longitudinal confocal microscopy imaging of solid tumor destruction following adoptive T cell transfer. *Oncoimmunology* **2**, e26677 (2013).

23. Hock, H. *et al*. Mechanisms of rejection induced by tumor cell targeted gene transfer of interleukin 2, interleukin 4, interleukin 7, tumor necrosis factor or interferon-gamma. *Proc. Natl. Acad. Sci. USA* **90**, 2774-2778 (1993).

24. Augustin, H.G. *et al*. Ovarian angiogenesis. Phenotypic characterization of endothelial cells in a physiological model of blood vessel growth and regression. *Am. J. Pathol*. **147**, 339-351 (1995).

25. Modlich, U. *et al*. Cyclic angiogenesis and blood vessel regression in the ovary: blood vessel regression during luteolysis involves endothelial cell detachment and vessel occlusion. *Lab. Invest*. **74**, 771-780 (1996).

26. Guo, S. *et al*. IRF4 is a novel mediator for neuronal survival in ischaemic stroke. *Cell Death Differ*. **21**, 888–903 (2014).

27. Rothstein, J. L. & Schreiber, H. Synergy between tumor necrosis factor and bacterial products causes hemorrhagic necrosis and lethal shock in normal mice. *Proc. Natl. Acad. Sci. USA* **85**, 607-611 (1988).

28. Johansson, A., Hamzah, J., Payne, C. J. & Ganss R. Tumor-targeted TNFα stabilizes tumor vessels and enhances active immunotherapy. *Proc. Natl. Acad. Sci. USA* **109**, 7841-7846 (2012).

Supplementary Information is available in the online version of the paper.

Acknowledgments

We thank R. Naumann, S. Jähne, T. Schüler, A. Sporbert, M. Richter, M. Schreiber, I. Gavvovidis, B. Purfürst, S. Fillatreau for support. This work was supported by the DFG through SFB-TR36 and the Einstein Stiftung Berlin.

Author contributions

TK and CF planned and performed most experiments. AA, CI, RW and HS generated and analysed imaging experiments. DBr established MCA313 cells. MR contributed ATT experiments. MLe contributed T cell experiments and performed retroviral gene transfer. SK generated and analysed transmission electron microscopy data. AT established 16.113-999 cells. GP and NH performed gene expression analysis. AI and DBe performed bioinformatics analysis. AS and HG advised and contributed HUVEC-experiments. DS, BE, and WU generated constructs. AH and HY performed 2-photon and VE-cadherin microscopy. HJF, MF and MLo provided mice. TB and TK conceived the project, analysed data and wrote the manuscript. All authors revised the manuscript.

Author Information Reprints and permissions information is available at www.nature.com/reprints. The authors declare no competing financial interests. Correspondence and requests for materials should be addressed to T.B.

Figure legends

Figure 1 | Reductionist model to identify the stromal target for IFNγ-induced tumour regression.

a, Experimental system consisting of IFNγR^{del} cancer cells, MCA313, with dox-inducible IFNγ expression (MCA313$^{IFNγ\text{-}IND}$) and transgenic mice with inducible IFNγR expression in defined cell types (PIG mice: Cre/LoxP-excision of stop-cassette allows CAG-promoter driven expression of IFNγR and GFP on an IFNγR^{del} genetic background). **b,** Dox-dependent IFNγ expression by MCA313$^{IFNγ\text{-}IND}$ cells *in vitro* (ELISA, mean and SD of 3 experiments). **c**, Similar IFNγ serum peak levels produced by MCA313$^{IFNγ\text{-}IND}$ (but not MCA313) tumours (peak day 2 after dox, tumours 790 ± 260 mm^3, filled circles, n = 9) and CD8$^+$ T cells during rejection of 16.113 tumours (peak day 4 after ATT, tumours 584 ± 153 mm^3, open circles, n = 16), mean ± s.e.m. **d - f**, Dox-induced IFNγ expression in MCA313$^{IFNγ\text{-}IND}$ tumours of PIG$^{Cmv\text{-}Cre}$ mice leads to **d,** necrosis (n = 2). **e,** blood vessel reduction (n = 2) within 120 h and **f,** tumour regression after dox application at a tumour size of 613 ± 467 mm^3 (n = 7). Combined data of 2 experiments. **g – i**, No effect as in **d - f** in control PIG$^{IFNγR\text{-}del}$ mice. **d** and **g,** size bar 0.5 cm. **i,** dox at a tumour size of 562 ± 65 mm^3 (n = 7). Combined data of 2 experiments. The number of mice, replications and sample size for each experiment are shown in Supplementary Table 3.

Figure 2 | IFNγ-responsiveness by endothelial cells is necessary and sufficient for necrosis, blood vessel reduction, and tumour regression by IFNγ.

Following IFNγ induction in MCA313$^{IFNγ\text{-}IND}$ tumours of (**a-c**) PIG$^{Lys\text{-}Cre}$ and (**d-f**) PIG$^{Fsp\text{-}Cre}$ mice, no necrosis, changes in blood vessel density (120 h after dox) or tumour regression was observed. **c, f**, Dox at a tumour size of 616 ± 183 mm^3 and 599 ± 175 mm^3, respectively (n = 7-8). Combined data of 2 experiments. **g - j,** To induce CreER-mediated recombination in endothelial cells, PIG$^{Pdgfb\text{-}Cre\text{-}IFNγ\text{-}del}$ mice received tamoxifen. **g**, necrosis and **h,** reduction in blood vessels 120 h after IFNγ induction. **i**, Tumour growth is delayed after IFNγ induction (right panel) in MCA313$^{IFNγ\text{-}IND}$ tumours (519 ± 30 mm^3, n = 6) grown in PIG$^{Pdgfb\text{-}Cre\text{-}IFNγ\text{-}del}$ mice compared to control mice (left panel). Starting day 21, tumour size differs significantly (**). **j**, Flowcytometry of tumour endothelial cells (CD31$^+$/CD146$^+$) of tumours depicted in **i,** shows that most endothelial cells in untreated tumours (app. day 20) are GFP$^+$, while most endothelial cells are GFP$^-$ in tumours after 48 ± 5 days IFNγ exposure. **k**, 10^7 tumour cells of indicated mice without (open bars) and 120 h after IFNγ induction (black bars), were analysed

for $CD31^+/CD146^+$ cells using flowcytometry. Size bar in **a, d, g,** 0.5 cm. Data are mean ± SD, ** $P<0.01$ and *** $P<0.001$. The number of mice, replications and sample size for each experiment are shown in Supplementary Table 3.

Figure 3 | Tumour ischemia versus tumour necrosis induced by intratumoural IFNγ-GFP or TNF-GFP fusion proteins, respectively.

a, IFNγ-GFP induction in cerulean$^+$ J558L$^{IFNγ\text{-}GFP\text{-}IND}$ cells 48 h after dox, analysed for IFNγ (ELISA, left y-axis and open bars) and GFP (flowcytometry, right y-axis and black bars). Mean ± SD of 3 experiments. **b**, Up-regulation of MHC-I on B16-F10 cells by IFNγ-GFP is comparable to recombinant IFNγ. Cells cultured with (black line) or without (dotted line) 1 ng/ml IFNγ (left panel) or IFNγ-GFP (right panel), were analysed for H-2K^b/H-2D^b expression (1 representative of 2 experiments). **c,** The same area of J558L$^{IFNγ\text{-}GFP\text{-}IND}$ tumours established for 12-14 days behind a glass window in Rag^{del} mice was repeatedly imaged over several days following dox. Shown: cancer cell viability (cerulean$^+$, 1st row), IFNγ-GFP expression (2nd row), vascular density (bright field, 3rd row) and blood flow (DiD-stained erythrocytes, 4th row) (see also Extended Data Fig. 8 and Supplementary Information Video 3). **d,** Quantification of changes in J558L$^{IFNγ\text{-}GFP\text{-}IND}$ tumour signal and blood vessel area over time. **e**, TNF-GFP induction in cerulean$^+$ J558L$^{TNF\text{-}GFP\text{-}IND}$ cells 48 h after dox, analysed as in **a** except for TNF ELISA (mean ± SD). **f,** Cytotoxicity of TNF-GFP towards L929 cells is comparable to recombinant TNF. L929 cells were exposed to titrated amounts of TNF-GFP or TNF, and viability was determined (XTT assay, OD at 450 nm). **f** mean of 2 experiments. **g,** J558L$^{TNF\text{-}GFP\text{-}IND}$ tumours imaged as in **c**. (see also Extended Data Fig. 7 and Supplementary Information Video 4). **h,** Quantification of changes in J558L$^{TNF\text{-}GFP\text{-}IND}$ tumour signal and blood vessel area over time. **d** and **h,** combined data (mean ± s.e.m.) of 2-5 areas per animal and time point of 3 mice with J558L$^{IFNγ\text{-}GFP\text{-}IND}$ and 4 mice with J558L$^{TNF\text{-}GFP\text{-}IND}$ tumours. The number of mice, replications and sample size for each experiment are also shown in Supplementary Table 3.

Material and Methods

Expression vectors

To construct the PIG (**p**CAG^{loxP}STOP^{loxP}-**I**FNγR-IRES-**G**FP) plasmid, the IRES-GFP sequence from pMIG[29] was excised with *HincII*. The resulting fragment was ligated into the blunt-ended *KpnI* site of pHMGmGIFR[30] resulting in pHMG-mIFNγR-IRES-GFP. To replace the LacZ gene of pCAG^{loxP}STOP^{loxP}Z[31] with the IFNγR-IRES-GFP fragment, pCAG^{loxP}STOP^{loxP}-Z was digested with *BamHI*, treated with Klenow fragment and thereafter the LacZ Gene was excised by digestion with *NotI*. Next, the IFNγR-IRES-GFP fragment was excised from pHMGmIFNγR-IRES-GFP using *SmaI* and *NotI* and was ligated into pCAG ^{loxP}STOP^{loxP} to generate **p**CAG^{loxP}STOP^{loxP}**I**FNγR-IRES-**G**FP.

The retroviral vector plasmid for inducible IFNγ expression, pMOV-IFNγ, has been described[19]. To obtain pMOV-IFNγ-GFP and pMOV-TNF-GFP, cDNA sequences encoding for GFP-tagged mIFNγ or mTNF, including a glycine-serine-linker $(G_4S)_3$ that is located between the cytokine and the GFP gene (replacing the cytokine 3' untranslated region), were de novo synthesized by GeneArt (Regensburg, Germany). The de novo synthesized sequences (IFNγ-GFP: 1230 bp, TNF-GFP: 1470 bp) contained *NotI* and *SalI* sites for ligation into *NotI* and *SalI* sites of pMOV.1-T2.

Mice

PIG mice were generated by excising the pCAG^{loxP}STOP^{loxP}IFNγR-IRES-GFP expression cassette using *KpnI* and *NotI*. The 8891 bp fragment was gel purified and injected into the pronucleus of fertilized C57BL/6 oocytes. C57BL/6, IFNγR^{del} (strain no. 003288), IFNγ^{del} (strain no. 002287), Rag1^{del} (strain no. 002216), Rag2^{del} (strain no. 008449) (referred to as Rag^{del}) and CMV-Cre mice (strain no. 006054) were obtained from the Jackson laboratories. TCR-I mice[32] are transgenic for a T-cell receptor specific for SV40 Large T, epitope I, and were obtained from Jackson laboratories (strain no. 005236) and crossed to a Rag^{del} genetic background. FSP-Cre mice[33] were provided by Eric G. Neilson (Northwestern University, Feinberg School of Medicine, Chicago) and were backcrossed for 10 generations to the C57BL/6 genetic background. Lys-Cre mice[34] backcrossed to C57BL/6 genetic background (N10) were obtained from Simon Fillatreau (German Centre for Rheumatology Research, Berlin). PDGFB-CreER-IRES-GFP mice[35] were backcrossed for 10 generations to the C57BL/6 genetic background. To obtain mice with cell type-specific expression of the IFNγR, PIG mice were crossed to the respective Cre strain (CMV-Cre, Lys-Cre, FSP-Cre,

PDGFB-CreER-IRES-GFP) and to IFNγR^{del} mice. PIG$^{IFNγR\text{-}del}$ x PDGFB-CreER-IRES-GFP were further crossed to IFNγ^{del} mice. Mice used in experiments were heterozygous for the PIG and Cre alleles and homozygous for the IFNγR^{del} (and IFNγ^{del}) allele. Rosa26-tdRFP mice were generated on the C57BL/6 genetic background[36] and were crossed to PDGFB-CreER-IRES-GFP mice. *Irf4^{del}* mice[37] were backcrossed for 10 generations to the C57BL/6 genetic background. *Irf4$^{wt/del}$* and *Irf4^{del}* were obtained by breeding *Irf4^{del}* male and *Irf4$^{wt/del}$* female mice. Male and female mice aged between 6 - 24 weeks were used and matched in experiments. All animal experiments were conducted in accordance with institutional, state, and federal guidelines and with permission of the local animal ethics committee of the LAGeSo, Berlin. Effect and sample size estimates were done and included in animal experiment applications. At any signs of illness (lethargy, hunched posture, scruffy coat, social isolation, inactivity or weight loss) mice were taken out of the experiment. All animals used for experiments are reported. No randomization was performed. No investigator blindfolding was performed for animal experiments.

Genotyping

The PIG transgene was identified by PCR with primers specific for the stop cassette (chloramphenicol acetyltransferase gene) 5'-CAG TCA GTT GCT CAA TGT ACC-3' and 5'-ACT GGT GAA ACT CAC CCA-3' and the GFP gene 5'-AAG TTC ATC TGC ACC ACC G-3' and 5'-TCC TTG AAG AAG ATG GTG CG-3'. The endogenous IFNγR gene was detected with a forward primer specific for exon 4: 5'-ATG CAA CGG TTT CCA CCC CC-3', and a reverse primer in intron 4: 5'-CCA GTC ATA GCC GAA TAG CC-3'. IFNγR^{del} gene was detected with a forward primer specific for exon 4 (as above) and a reverse primer specific for the neomycin resistance gene 5'-CCA CCT CAG CAC TGT CTT CA-3'. IFNγ^{del} mice were genotyped using the primers: oIMR6218 5'-CCT TCT ATC GCC TTC TTG ACG-3', oIMR8284 5'-AGA AGT AAG TGG AAG GGC CCA GAA G-3' and oIMR8285 5'-AGG GAA ACT GGG AGA GGA GAA ATA T-3'. Rosa26-RFP mice were genotyped by PCR using primers 5'-AAG ACC GCG AAG AGT TTG TCC-3', 5'-TAA GCC TGC CCA GAA GAC TCC-3' and 5'-AAG GGA GCT GCA GTG GAG TA-3'. The PDGFB-CreER-IRES-GFP transgene was detected using primers 5'-GCC GCC GGG ATC ACT CTC G-3' and 5'-CCA GCC GCC GTC GCA ACT C-3'. All other Cre-transgenic mice (Lys-Cre, FSP-Cre and CMV-Cre) were genotyped by using the generic Cre-PCR from the Jackson labs with the primers: oIMR1084 5'-GCG GTC TGG CAG TAA AAA CTA TC-3' and oIMR1085 5'-GTG AAA CAG CAT TGC TGT CAC TT-3'. The genotype of, Rag^{del}, TCR-I mice was confirmed

by flowcytometry of PBMC for T cells B cells (Rag^{del} and TCR-I) or for hematopoietic cells. The genotype for PIG x CMV-Cre, Lys-Cre, FSP-Cre, PDGFB-CreER-IRES-GFP was confirmed by flowcytometry assessing GFP. $Irf4^{del}$ mice are unable to generate IgM, therefore lack of serum IgM (determined by ELISA) classified $irf4^{del}$ animals.

Cells

MCA313 is a fibrosarcoma that was induced by s.c. injection of 25 μg methylcholanthrene (MCA) dissolved in sesame oil in an $IFN\gamma R^{del}$ mouse. $MCA313^{IFN\gamma\text{-}IND}$ and $16.113\text{-}999^{IFN\gamma\text{-}IND}$ cells were generated by retroviral transduction with pMOV-IFNγ by standard procedures[19]. Cells were cloned by limiting dilution and selected for optimal IFNγ induction and no expression in the absence of dox. J558L is a BALB/c-derived plasmacytoma cell line. $J558L^{TNF\text{-}GFP\text{-}IND}$ and $J558L^{IFN\gamma\text{-}GFP\text{-}IND}$ cells were generated by retroviral transduction of J558L cells with pMOV-IFNγ-GFP or pMOV-TNF-GFP, cloned and selected as described above. $J558L^{TNF\text{-}GFP\text{-}IND}$ and $J558L^{IFN\gamma\text{-}GFP\text{-}IND}$ cells were additionally transduced with the retroviral vector pMFG-Cerulean[22]. B16-F10 is a mouse melanoma cell line isolated from C57BL/6 mice and L929 is a fibrosacroma cell line derived from a C3H/An mouse. 16.113 is a carcinoma cell line derived from the colon of LoxP-Tag mice[38]. 16.113-999 is an IFNγ−insensitive variant of 16.113 cell line[39]. All cell lines mentioned above were cultured in RPMI 1640 Medium with 10% FCS. Send.1 cells are polyoma middle T antigen immortalized endothelial cells from blood vessels of the skin. Send.1 cells were cultured in Dulbecco's modified Eagle's medium DMEM with 20% FCS. Fibroblasts were generated by cutting tail skin into small pieces and digesting them overnight in DMEM, 20% FCS containing collagenase II (1 mg/ml) and dispase (1 mg/ml) at 37 °C. Digestion was stopped by changing the medium (DMEM, 10% FCS). To generate immortalized fibroblasts from PIG mice, primary fibroblast cultures were transfected with the plasmid pCMV-Tagori[40] and with the plasmid pBabe-puro using Lipofectamine 2000 (Life Technologies) according to the manufacturer's instruction. Transfected fibroblasts were selected using 1 μg/ml puromycin. To rule out bacterial products synergising with TNF, J558L cells were negatively tested for the presence of mycoplasma by PCR using the Primers: 5'-TGC ACC ATG TGT CAC TCT GTT AAC CTC-3' and 5'-GGG AGC AAA CAG GAT TAG ATA CCC T-3'. No commonly misidentified cell line was used in the study. MCA313 are fibrosarcoma, J558L plasmocytoma and 16.113 are carcinoma cells that were distinguished by morphology in cell culture. No other authentication was used.

Culture and imaging of HUVECs

Donor-pooled human umbilical vein endothelial cells (HUVECs, PromoCell, GmbH) were cultured in Endothelial Growth Medium 2 (Lonza, Ltd) according to manufacturer's instructions for a maximum of 5 passages. For immunofluorescence and time lapse experiments, cells were plated on 18 mm coverslips or in Nunc Lab-Tek chambered coverglass #1.5 (ThermoFisher Scientific, Inc.) coated with 10 µg/ml bovine plasma fibronectin (Sigma-Aldrich, Co. Llc. cat. # F1141). Cells were treated with recombinant human IFNγ (PeproTech) every 24 h for a total of 4 days. In order to stain actin filaments for live cell experiments, 250 nM SiR-Actin was added to the cells 1 hour before the start of the imaging. For immunofluorescence analysis of HUVECs, cells were fixed and permeabilized for 1 min. with 0.3% glutaraldehyde (EM Grade, Electron Microscopy Sciences), 0.25% Triton X-100 in cytoskeleton buffer (CB: 10 mM MES pH 6.1, 150 mM NaCl, 5 mM EGTA, 5 mM glucose, 5 mM $MgCl_2$) followed by a second fixation step with 2% paraformaldehyde (Electron Microscopy Sciences) in CB for 10 min. The sample was quenched with 0.1% $NaBrH_4$ for 7 min. and washed thrice with PBS for 10 min. The sample was incubated in blocking buffer (3% BSA in PBS) for 1 h and stained overnight with rabbit polyclonal anti-human VE-cadherin antibody (Abcam, # ab33168) in blocking buffer. The sample was then incubated for 1 h with donkey anti-rabbit IgG conjugated to Alexa Fluor 647 and 250 nM phalloidin conjugated to Alexa Fluor 488 (ThermoFisher Scientific, Inc). Samples were mounted in Abberior Mount Solid mounting media (Abberior, GmbH). Imaging of HUVECs was performed on LSM 780 confocal microscope with Plan Apochromat 63x NA 1.4 Oil objective (Carl Zeiss). Time-lapse series with reflection-based autofocus were acquired using a custom written Visual Basic macro (Antonio Politi and Jan Ellenberg, EMBL Heidelberg), acquiring at least three positions per experiment per condition. Z-stacks covering the entire cell volume were acquired and maximum intensity projected. Live imaging was performed at 37 °C under 5% CO_2.

Cytokine analysis

2 x 10^5 $MCA313^{IFN\gamma\text{-}IND}$, $J558L^{TNF\text{-}GFP\text{-}IND}$ or $J558L^{IFN\gamma\text{-}GFP\text{-}IND}$ cells/ml were cultured for 48 h without or in the presence of 10, 50, or 100 ng/ml dox (Sigma Aldrich). Culture supernatants were analysed by IFNγ- or TNF-specific ELISA according to the manufacturer's (OptEIA™; BD Biosciences) recommendation. TNF biological activity of the TNF-GFP fusion protein was analysed by an L929 cytotoxicity assay. L929 cells were seeded at 3.5 x 10^4 cells in 96 wells in RPMI, 2% FCS and cultured overnight. Then, 2 µg/ml Actinomycin D (Sigma

Aldrich) and recombinant TNF (Peprotech) or TNF-GFP in concentrations as indicated were added in fresh medium (RPMI, 2% FCS) and incubated for 24 h. Thereafter, fresh XTT (sodium,2,3,-bis(2-methoxy-4-nitro-5-sulfophenyl)-5-[(phenylamino)-carbonyl]-2H-tetrazolium) solution was added, incubated for 4 h, and absorbance was measured at 450 nm. For each concentration, 3 replicates were tested per plate. To evaluate the bioactivity of the IFNγ-GFP fusion protein, 10^6 B16-F10 cells were cultured in 5 ml RPMI 1640 medium 10% FCS containing either recombinant IFNγ or IFNγ-GFP at a concentration of 1 ng/ml. After 48 h, MHC-I up-regulation was analysed by flowcytometry. Blood samples were collected from the facial vein using a sterile lancet. Blood was allowed to agglutinate and then centrifuged for 20 min. at 4 °C. Serum samples were aliquoted and stored at -80 °C. To determine serum IFNγ levels, 20 µl serum were analysed using the cytometric bead array from eBioscience (Procartaplex) according to manufacturer's instructions.

Tumour experiments

10^6 MCA313$^{IFN\gamma\text{-}IND}$ cells, 16.113-999$^{IFN\gamma\text{-}IND}$, J558L$^{TNF\text{-}GFP\text{-}IND}$ or J558L$^{IFN\gamma\text{-}GFP\text{-}IND}$ cells were injected s.c. into the right flank of the mice. Tumours were measured 2-3 times weekly in three perpendicular diameters using a calliper and tumour volume was calculated using the ellipsoid volume formula ($\pi/6$ x a x b x c). According to the animal application approved by the local ethics committee (LAGeSo Berlin), animals were taken out of the experiment, if tumours reached an average diameter of 1.5-2 cm. In none of the experiments, a tumour reached a larger size. Mice with tumour necrosis were observed daily and monitored for humane endpoint criteria (lethargy, hunched posture, scruffy coat, social isolation, inactivity or weight loss) and in no case any of those exclusion criteria were detected. Dox was continuously administered by adding 1 mg/ml dox to light-protected drinking water (supplemented with 20 mg/ml glucose). Tamoxifen was administered via the chow at 400 mg/kg (TAM400, LASvendi) three days before tumour cell transplantation as indicated. Before mice were exposed to tamoxifen chow, they were administered for 10 days soy-free chow from LASvendi to exclude effects from phytoestrogens.

In experiments described in Fig. 1f and Extended Data Fig. 1a (left panel), dox was administered in 48 h intervals (48 h on dox, 48 h on water). In intravital imaging experiments, dox was administered by daily bolus injection of 10 µg i.p. For adoptive T-cell therapy, 10^6 16.113 cells were s.c. injected into Rag^{del} mice. When tumours were established (approximately 500 mm^3), mice received 10^7 TCR-I T cells from Rag^{del} x TCR-I mice i.v. per animal at the indicated time point. In the experiment described in the Extended Data Fig. 1h,

T cells from C57Bl/6 or IFNγ^{del} mice were transduced with a retroviral vector to express the TCR-I T cell receptor. 5 days after ATT with 10^6 TCR-I-transduced T cells, tumours were isolated and after tissue digestion the number of endothelial cells was analysed by flowcytometry.

For experiments in Extended Data Fig, 3d, Rag^{del} mice or Rag^{del} x IFNγR^{del} mice were reconstituted with 2 x 10^7 splenocytes from WT mice. Two weeks after T cell transfer, 10^6 MCA313$^{IFNγ\text{-}IND}$ cells were injected and when tumours were established (846 ± 263 mm^3), IFNγ was induced. 5 days after IFNγ induction tumours were isolated and after tissue digestion endothelial cells (CD31 and CD146 double positive cells) from 10^7 tumour cells were analysed by flowcytometry.

Potential immunogenicity of transgenes used in this study was excluded by experiments showing that MCA313$^{IFNγ\text{-}IND}$ tumours grew and regressed after IFNγ induction with the same kinetics in WT and Rag^{del} mice (Extended Data Figure 1a) and, furthermore, cells expressing the rtTA protein were not eliminated even after 100 days in fully immunocompetent mice (Extended Data Figure 5f).

Wound healing experiments

10^6 MCA313$^{IFNγ\text{-}IND}$ cells were injected s.c. into the right flank of indicated mice. After one week (tumour size approximately 50 mm^3), mice were anesthetized, and a wound of 5 mm in diameter was instilled on the back of the mice using a biopsy punch. For the first 48 h, analgesia was administered. Mice were inspected every day. The wound healing process was recorded by taking photos and by measuring the diameter of the wound in two perpendicular axes using a calliper.

Gene expression analysis

Tumour endothelial cells (CD31$^+$/CD146$^+$) were isolated by fluorescence-activated cell sorting into RNAzol®. cDNA was synthesized from ~500 pg total RNA according to the standard Affymetrix protocol GeneChip® WT Pico Kit (P/N # 902623) by using the Affymetrix T7 RNA polymerase promoter which is attached to random primers. Pre-IVT was performed with 12 amplification cycles. Then, ss-cDNA was fragmented and biotin-labelled according to Affymetrix recommendations. Fragmented cDNA (3.8 µg) was hybridized to MOGENE 2.0 ST arrays. Arrays were washed and stained in the Affymetrix Fluidics Station 450 and further scanned using the Affymetrix GeneChip® Scanner 3000 7G. Software: Affymetrix GeneChip Command Console Version 4.0. The image data were normalized and

quality controlled with the Affymetrix Expression Console™ Software Version 1.4. The microarray data were deposited in the GEO data repository under the accession number GSE94504.

The bioinformatics analysis of the gene expression data was carried out with R BioConductor, to quantify the gene expression changes and normalize array intensity values for the comparison between the samples we used "rma" function from "oligo" package (target="probeset" parameter was used). Manufacturer's probe identifiers were converted to mouse gene names with "mogene20stprobeset.db" annotation. After background subtraction and quantile normalization each gene intensity is determined as median of probe set intensities. Log fold changes are computed from the average across replicates. For MCA313$^{IFN\gamma\text{-}IND}$ data from 24 h and 48 h after induction were so consistent that they could be regarded as replicates (data not shown). Differential expression analysis was carried out with "limma" package by computing moderated t-statistics and Benjamini-Hochberg adjusted P-values. Number of replicates (rep.) analysed were: MCA313$^{IFN\gamma\text{-}IND}$ 0 h 3-rep., MCA313$^{IFN\gamma\text{-}IND}$ 24 h 2-rep., MCA313$^{IFN\gamma\text{-}IND}$ 48 h 2-rep., J558L$^{IFN\gamma\text{-}GFP\text{-}IND}$ 0 h 3-rep., J558L $^{IFN\gamma\text{-}GFP\text{-}IND}$ 24 h 2-rep., normal kidney 0 h 3-rep., normal kidney 24 h 3-rep. WT T cells 5 days 3-rep., IFNγ^{del} T cells 5 days 5-rep.

Longitudinal imaging using window chambers

The procedure to surgically implant window chambers and perform longitudinal imaging is detailed elsewhere[22]. In short, window chambers were implanted into mice, and mice were injected with 10^6 cancer cells. 13-18 days later, dox administration was started and continued throughout the experiment. For microscopic analysis, mice with window chambers were anesthetized using isofluorane. The window was fastened to the main stage of the microscope using a custom-made holder. The microscope (Leica SP5 II TCS Tandem scanner 2-photon spectral confocal with 4 x and 20 x /0.45 LWD IR objectives from Olympus) has a heated chamber for maintaining body temperature. The software and X-Y motorized stage allow returning to memorized positions within the window at later times. For visualization of the tumour vasculature and blood flow, mice were injected with 1,1-dioctadecyl-3,3,3,3-tetramethylindodicarbocyanine perchlorate (DiD)-labeled red blood cells (RBC). Briefly, RBC were obtained from the peripheral blood of Rag^{del} mice and labelled with DiD (Invitrogen) for 30 min. at 37 °C. After 3 washes with PBS, DiD-labeled RBC were injected intravenously. Absorption and fluorescence emission maxima of DiD are 644 nm and 665 nm

respectively. The optical penetration of tissue typically ranged between 100-150 µm. The acquired images were analysed using Fiji[41].

Intravital 2-photon microscopy

24 h prior to imaging procedure, 10 µg dox was injected i.p. in 100 µl PBS. *In vivo* multiphoton microscopy (IVMPM) of J558L$^{IFN\gamma\text{-}GFP\text{-}IND}$ tumours engrafted in Rag^{del} mice was performed while mice were anaesthetized with isoflurane. For IVMPM, an Ultima Multiphoton Microscopy System was used (Prairie Technologies). For imaging GFP, the excitation wavelength was set to l = 890 nm. Band-pass filters optimized for GFP (BP l = 525/50 nm) were used for detection. Collected single plane images were assembled to a 3D stack for each tumour *in silico* using Amira 3D software.

Transmission electron microscopy

Tumour tissue was fixed by immersion in phosphate buffered 4% (w/v) paraformaldehyde and 1.25% (v/v) glutaraldehyde. Samples were postfixed with 1% (v/v) osmium tetroxide, dehydrated in a graded series of ethanol, and embedded in the PolyBed® 812 resin (Polysciences, Inc., Germany).

Ultrathin sections (60-80 nm) were stained with uranyl acetate and lead citrate, and examined at 80 kV with a Zeiss EM 910 electron microscope (Zeiss, Oberkochen, Germany). Acquisition was done with a Quemesa CDD camera and the iTEM software (Emsis GmbH, Germany) and pictures were processed using Adobe Illustrator.

Antibodies and staining reagents

The following anti-mouse antibodies were used for flowcytometry: NK1.1 (clone PK136, Miltenyi Biotec # 130-102-400, isotype control mouse IgG2a # 130-091-835), CD8 (clone 53-6.7, Biolegend # 100712, # 100708, isotype control rat IgG2a # 400508, # 400512), CD4 (clone RM4-4, Biolegend # 116014, # 116006, isotype control rat IgG2b # 400612, # 400608), CD3 (clone 145-2C11, Biolegend # 100336, isotype control Armenian hamster IgG # 400935), CD19 (clone 6D5, Biolegend # 115512, 115508, isotype control rat IgG2a # 400512, # 400508), CD11b (clone M1/70, Biolegend # 101216, isotype control rat IgG2b # 400618), GR-1 (Clone RB6-8C5, Biolegend # 108424, isotype control rat IgG2b # 400624), CD11c (clone N418, Biolegend # 117329, # 117308, isotype control Armenian hamster IgG # 400935, # 400908), F4/80 (clone BM8, Biolegend # 123110, isotype control rat IgG2a # 400508), CD119 (clone 2E2, Biolegend # 112804, isotype control Armenian hamster IgG #

400903), CD119 (clone 2E2, BD # 550482, isotype control Armenian hamster IgG1 # 553970), CD31 (clone 390, eBioscience # 25-0311-82, Biolegend # 102418, isotype control rat IgG2a, k # 400522), CD146 (clone ME-9F1, Biolegend # 134704, isotype control rat IgG2a # 400508), CD146 (clone ME-9F1, Miltenyi Biotec # 130-102-739, isotype control rat IgG2a # 130-102-652), CD45.2 (clone 104-2, Miltenyi Biotec # 130-102-980, # 130-102-355, isotype control mouse IgG2a # 130-098-898). Further reagents used for flowcytometry: viability dye eFluor® 450 or eFluor® 660 (eBioscience # 65-0863-18, # 65-0864-18), Faser-kit APC (Miltenyi Biotec # 130-091-762), streptavidin-APC (Biolegend # 405207), 7-aminoactinomycin (7AAD) (Biolegend # 420404). The following anti-mouse antibodies were used for confocal and fluorescence microscopy: GFP (Invitrogen # A-11122), CD11b (clone M1/70, abcam # 8788, isotype control rat IgG2b # ab18450), FAP (rabbit polyclonal IgG, abcam # 53066,), CD31 (clone MEC13.3, BD # 550274, isotype control rat IgG2a # 553894), CD146 (clone ME9-F1, Biolegend # 134702, isotype control rat IgG2a # 400501) and F480 (BM8, Biolegend # 123102, isotype control rat IgG2a # 400501), ERG (abcam # 196149, isotype # 199093), cleaved caspase 3 (cell signalling # 9604S), collagen 4 (AbD Serotec # 2150-1470). As secondary antibodies Alexa 488- (# A21206), Alexa 594- (# A21207 and # A21209), Alexa 568 (# A11077) - and Alexa 647- (# A31573 and # A21472) labelled: anti-rat IgG and anti-rabbit IgG (Life Technologies) were used. Hoechst 33342 was used for staining nuclei.

Flowcytometry

To analyse PBMC, blood was taken from the facial vein using a sterile lancet. Erythrocytes were lysed using ACK lysis buffer (BD Biosciences). To exclude dead cells from analysis, 7-AAD or the fixable viability dye eFluor® 450 were used. For staining of tumour stroma cells, tumours were isolated, cut into small pieces and digested for 1 h in RPMI 1640 medium containing 10 mg/ml collagenase II, 10 mg/ml dispase and 10 µg/ml DNase I. Cells were washed in PBS and filtered over a 40 µm nylon mesh. Fc-receptors were blocked with anti-CD16/32 blocking antibodies. To analyse tumour endothelial cells, we used an integrated magnetic enrichment, using anti-PE magnetic microbeads that were added to the sample of PE-positive cells (stained with CD31-PE-Cy7 / CD146-PE) and were directly enriched before FACS analysis, as suggested for analysis of rare cells when using the MACSQuant analyser. 10^7 total cells from digested tumour material were stained with CD45.2, CD31, CD146 and live/dead cell exclusion. For IFNγR (CD119) staining, a biotin-labelled anti-CD119 (2E2) antibody in combination with streptavidin-APC was used, the signal was subsequently

enhanced by amplification using the FASER Kit-APC (Miltenyi Biotec) using streptavidin-anti-APC antibodies. Control staining was done without the primary antibody. For intracellular staining of IRF4, anti-IRF4 mAb (Biolegend # 646408) and the transcription factor staining kit (eBioscience # 00-5523) was used.

Nitric oxide synthase assay

For isolating macrophages, tumours were cut into small pieces and digested as described above. Cells were washed in PBS and filtered over a 40 µm nylon mesh and labelled with anti-mouse CD11b MACS beads (Miltenyi Biotec). CD11b cells were purified by magnetic cell sorting (purity was > 90%). 4 x 10^5 CD11b cells were seeded in 12 well tissue culture plates. Cells were stimulated with 250 U/ml IFNγ for 24 h. The nitrite ion was measured in a Griess diazotization reaction using Griess reagent system (Promega) according to the manufacturer's instructions. In short, 50 µl of medium was mixed with 50 µl of sulfanilamid solution and incubated for 10 min. protected from light. Next, Griess reagent (N-(1-Naphthyl)ethylenediamine) was added and incubated for another 10 min. protected from light. Thereafter, absorbance was measured at 540 nm. NO concentration was determined using the OD value from the NO standard curve and medium without standard (blank) was set as detection limit.

Immunohistochemistry

Tumour tissues were fixed in 4% paraformaldehyde (Sigma Aldrich) containing 10% m/w sucrose overnight, incubated overnight in PBS-sucrose solution (25% m/w) and embedded in OCT-tissue tech (Sakura). 5 µm sections were mounted on slides. Slides were treated with 0.2% galantine (Sigma Aldrich) and 0.2% Triton X-100 in PBS and additionally blocked with antibody diluent (Dako) for 1 h at RT. All antibody staining were performed in Dako antibody diluent solution. Primary antibodies were incubated overnight at 4 °C. After 3 times washing with PBS, 2nd antibodies were added for 1 h together with Hoechst 33342 (Sigma Aldrich) at room temperature. Negative controls were generated by staining with the 2nd antibodies and Hoechst 33342 only. After staining, the slides were covered with slowfade (Life Technologies) and analysed with ObserverD.1 or LSM710 confocal microscopes (Zeiss). H&E staining were performed on 5 µm paraffin embedded tissue sections. After de-paraffinization and rehydration, sections were stained with haematoxylin (Gill no. 2) and eosin and covered with histomout and examined under an OberserverD.1 microscope with Zen software. For evaluation of erythrocytes, eosin fluorescence signals were captured and at

least 60 high magnification fields from 3-4 tumours were analysed for each experimental group. Analysis was performed using ZEN software (Zeiss), ImageJ (version 1.49) or Imaris.
For VE-cadherin staining of tumour vasculature tissue sections were fixed using 2% paraformaldehyde in PBS for 15 min. at RT followed by three washes for 5 min. with PBS and 10 min. incubation in ice-cold methanol and another three washes for 5 min. with PBS. Image IT enhancer was employed for 30 min at RT followed rinsing in PBS and one wash for 5 min with PBS. Blocking solution (PBS containing 10% goat serum and 2.5% mouse serum; Sigma) was used for 1 h at RT before staining procedure was started using anti-CD31 and anti-VE-cadherin (eBioscience # 14-1441-82) diluted 1:50 in blocking solution incubated on tissue sections over night at 4 °C in a wet chamber. Secondary antibodies diluted 1:100 in blocking solution containing Hoechst 33342 were incubated for 2-3 hours at RT. Mowiol was used as mounting medium after three finalizing washing steps with PBS for 5 min at RT.

Statistics

To estimate the effect size for those experiments not involving animals and presented in the paper, one pilot experiment was performed. Then, usually a second experiment powered on what was observed in the pilot experiment was performed to attain significance and to test reproducibility. Data in general met the assumptions of the tests performed. The variance was in general similar between the groups that were being statistically compared and data met the assumptions of the tests. Statistical analysis was performed with GraphPad Prism 5.0. When comparing two groups if not indicated otherwise, we used the two tailed Mann-Whitney-U-Test. When comparing more than two groups, we used the one-way ANOVA test. p values less than 0.05 were considered as significant, * $P<0.05$, ** $P<0.01$ and *** $P<0.001$.

Data availability

The datasets generated during the current study are available from the corresponding author on reasonable request. The custom written AFS Visual Basic macro for the time-lapse microscopy series with reflection based autofocus was developed by Antonio Politi and Jan Ellenberg (EMBL Heidelberg) and is available at http://www.ellenberg.embl.de/. The microarray data are available from the GEO data repository under the accession number GSE94504.

29 Refaeli, Y., Van Parijs, L., Alexander, S. I. & Abbas, A. K. Interferon gamma is required for activation-induced death of T lymphocytes. *J. Exp. Med.* **196**, 999-1005 (2002).

30 Hemmi, S. *et al.* Cloning of murine interferon gamma receptor cDNA: expression in human cells mediates high-affinity binding but is not sufficient to confer sensitivity to murine interferon gamma. *Proc. Natl Acad. Sci. U S A* **86**, 9901-9905 (1989).

31 Sakai, K., Mitani, K. & Miyazaki, J. Efficient regulation of gene expression by adenovirus vector-mediated delivery of the CRE recombinase. *Biochem. Biophys. Res. Commun.* **217**, 393-401 (1995).

32 Staveley-O'Carroll, K. *et al.* In vivo ligation of CD40 enhances priming against the endogenous tumor antigen and promotes CD8+ T cell effector function in SV40 T antigen transgenic mice. *J. Immunol.* **171**, 697-707 (2003).

33 Bhowmick, N. A. *et al.* TGF-beta signaling in fibroblasts modulates the oncogenic potential of adjacent epithelia. *Science* **303**, 848-851 (2004).

34 Clausen, B. E., Burkhardt, C., Reith, W., Renkawitz, R. & Forster, I. Conditional gene targeting in macrophages and granulocytes using LysMcre mice. *Transgenic Res.* **8**, 265-277 (1999).

35 Claxton, S. *et al.* Efficient, inducible Cre-recombinase activation in vascular endothelium. *Genesis* **46**, 74-80 (2008).

36 Luche, H., Weber, O., Nageswara Rao, T., Blum, C. & Fehling, H. J. Faithful activation of an extra-bright red fluorescent protein in "knock-in" Cre-reporter mice ideally suited for lineage tracing studies. *Eur. J. Immunol.* **37**, 43-53 (2007).

37 Mittrücker H. W. Requirement for the transcription factor LSIRF/IRF4 for mature B and T lymphocyte function. *Science* **275**, 540-543 (1997).

38 Willimsky, G. & Blankenstein, T. Sporadic immunogenic tumours avoid destruction by inducing T-cell tolerance. *Nature* **437**, 141-146 (2005).

39 Textor A. W. *et al.* Preventing tumor escape by targeting a post-proteasomal trimming independent epitope. *J. Exp. Med.* **213**, 2333-2348 (2016).

40 Li, L. P., Schlag, P. M. & Blankenstein, T. Transient expression of SV 40 large T antigen by Cre/LoxP-mediated site-specific deletion in primary human tumor cells. *Hum. Gene Ther.* **8**, 1695-1700 (1997).

41 Schindelin, J. *et al.* Fiji: an open-source platform for biological-image analysis. *Nat. Methods* **9**, 676-682 (2012).

Extended Data Figures

Tumour ischemia by IFNγ resembles physiological blood vessel regression

Thomas Kammertoens, Christian Friese, Ainhoa Arina, Christian Idel, Dana Briesemeister, Michael Rothe, Andranik Ivanov, Anna Szymborska, Giannino Patone, Severine Kunz, Daniel Sommermeyer, Boris Engels, Matthias Leisegang, Ana Textor, Hans Joerg Fehling, Marcus Fruttiger, Michael Lohoff, Andreas Herrmann, Hua Yu, Ralph Weichselbaum, Wolfgang Uckert, Norbert Hübner, Holger Gerhard, Dieter Beule, Hans Schreiber, and Thomas Blankenstein

Extended Data Figure 1: Release of IFNγ in established tumours leads to necrosis, tumour blood vessel reduction and tumour regression.

Extended Data Figure 2: Mice with conditional IFNγR expression.

Extended Data Figure 3: Cre-mediated recombination induces GFP expression in myeloid or in myeloid and fibroblastoid stroma cells of MCA313$^{IFNγ\text{-}IND}$ tumours in PIG$^{Lys\text{-}Cre}$ mice and in PIG$^{Fsp\text{-}Cre}$ mice respectively and IFNγ signalling in T cells does not contribute to reduction in CD31^{+}/CD146^{+} tumour endothelial cells after IFNγ induction in established tumours.

Extended Data Figure 4: Tamoxifen-induced, Cre-mediated recombination in MCA313$^{IFNγ\text{-}IND}$ tumour endothelial cells of PDGFB-CreER-IRES-GFP x Rosa26-RFP mice and IFNγ-competent mice with IFNγR expression exclusively in endothelial cells show necrosis before IFNγ induction, but further reduction in blood vessel density and tumour regression after IFNγ induction.

Extended Data Figure 5: GFP and IFNγR are expressed in MCA313$^{IFNγ\text{-}IND}$ tumour endothelial cells of PIG$^{Pdgfb\text{-}Cre\text{-}IFNγ\text{-}del}$ mice. Tumours progressing after prolonged IFNγ exposure in these mice are largely necrotic but still produce IFNγ and wound healing is impaired in PIG$^{Pdgfb\text{-}Cre\text{-}IFNγ\text{-}del}$ mice.

Extended Data Figure 6: Induction of IFNγ-GFP fusion protein induces regression of established J558L$^{IFNγ\text{-}GFP\text{-}IND}$ tumours and blood vessels.

Extended Data Figure 7: Induction of TNF-GFP fusion protein induces regression of established J558L$^{TNF\text{-}GFP\text{-}IND}$ tumours and bursting of blood vessels.

Extended Data Figure 8: Erythrocyte extravasation after induction of TNF-GFP but not IFNγ-GFP.

Extended Data Figure 9: Activated blood vessels but not normal vessels regress upon IFNγ exposure and regression is accelerated in Irf4^{del} mice. IFNγ derived from T cells induces similar changes in gene expression as IFNγ from J558L$^{IFNγ\text{-}GFP\text{-}IND}$ or MCA313$^{IFNγ\text{-}IND}$ cells.

Extended Data Figure 10: IFNγ-mediated blood vessel regression in MCA313$^{IFNγ\text{-}IND}$ tumours in PIG$^{Pdgfb\text{-}Cre\text{-}IFNγ\text{-}del}$ mice.

Extended Data Figure 1 | Release of IFNγ in established tumours leads to necrosis, blood vessel reduction and tumour regression. a-c, MCA313$^{IFNγ-IND}$ tumours **d, h,** 16.113 tumours and **e-g** 16.113-999$^{IFNγ-IND}$ tumours. **a,** Without IFNγ induction, MCA313$^{IFNγ-IND}$ tumours grow progressively (1st panel). Dox-induced IFNγ expression in established MCA313$^{IFNγ-IND}$ tumours (2nd panel) leads to tumour regression in WT but not IFNγR^{del} mice (3rd, 4th panel). Differences in tumour growth between "no dox" and "dox" groups in WT mice are statistically significant on days 19 (*) 23 (**) and 25 (***). IFNγ induction in WT mice at 642 ± 236 mm^3 (the 2 crosses indicate mice that reached a humane endpoint and were taken out of the experiment) and in IFNγR^{del} mice at 608 ± 130 mm^3. No difference in tumour growth and IFNγ-induced tumour regression of MCA313$^{IFNγ-IND}$ tumours between Rag^{del} and Rag-competent hosts (5th panel Rag^{del}, n = 5, and 6th panel WT, n = 6). Dox administration at 1304 ± 290 mm^3 on day 15. **b, c,** MCA313$^{IFNγ-IND}$ tumours without and 120 h after dox. **b,** Macroscopic image size bar 0.5 cm, and **c,** H&E staining (1st row), N and dotted line indicate necrotic area, (2nd row) immunohistology using anti-CD31 mAb, size bars 100 µm. **c,** For H&E staining 3 animals per group with 4 to 5 areas were compared and differences are statistically significant (***). **d,** T cell-mediated rejection of 16.113 tumours. Mice (same as depicted in Figure 1c) were s.c. injected with 10^6 16.113 cells. On day 57, 10^7 TCR transgenic T cells specific for SV40-Large T, epitope I (TCR-I), expressed by 16.113 tumour cells, were transferred when tumour size was 489 ± 253 mm³. Combined data from two experiments is shown (n = 16). **e-g,** Induction of IFNγ in established carcinomas leads to tumour regression and blood vessel reduction. **e,** Dox-dependent IFNγ expression by 16.113-999$^{IFNγ-IND}$ cells in vitro, analysed by ELISA (mean values from two experiments are shown). **f,** Dox-induced IFNγ expression in established 16.113-999$^{IFNγ-IND}$ tumours grown in Rag^{del} mice leads to tumour regression and **g,** blood vessel reduction. The relative number of tumour endothelial cells (CD31$^+$/CD146$^+$) without and 120 h after IFNγ induction in tumours was determined from 10^7 tumour cells by flowcytometry. **h**, IFNγ released during T cell-mediated rejection of 16.113 tumours contributes to blood vessel reduction. Tumours were established as in **d**, and either not treated, treated with 10^6 TCR-I transduced T cells from either WT or IFNγ^{del} mice. On day 5 after ATT, the relative number of tumour endothelial cells (CD31$^+$/CD146$^+$) was determined as in **g**. * *P*<0.05, ** *P*<0.01 and *** *P*<0.001.The number of mice, replications and sample size for each experiment are shown in Supplementary Table 3.

Extended Data Figure 2 | Mice with conditional IFNγR expression. a, Schematic representation of transgenes combined to generate mice with conditional IFNγR expression. **b** and **c,** Functional IFNγR expression in PIG$^{IFNγR-del}$ fibroblasts upon Cre-mediated excision of the stop cassette. **b**, Immortalized tail fibroblasts from PIG$^{IFNγR-del}$ mice were transfected with pBabe-puro-Cre plasmid, selected for puromycin resistance and analysed for GFP and IFNγR (CD119) expression by flowcytometry. WT fibroblasts served as control. One representative out of 2 experiments is shown. **c,** IFNγ induces MHC I up-regulation in Cre-transfected fibroblasts from PIG$^{IFNγR-del}$ mice. Flowcytometry of MHC I expression by fibroblasts from PIG$^{IFNγR-del}$ mice with (right panel) or without Cre-transfection (middle panel) (same fibroblasts as shown in b) that were cultured without (dotted line) or with 1 ng/ml IFNγ for 48 h (black line). Fibroblasts from WT mice served as control (left panel). One representative out of 2 experiments is shown. **d, e,** Cre-mediated recombination induces GFP expression in tumour stroma cells of PIG$^{Cmv-Cre}$, shown by immunohistology. MCA313$^{IFNγ-IND}$ tumours from **d,** PIG$^{Cmv-Cre}$ and **e**, PIG$^{IFNγR-del}$ mice. GFP signals were amplified by anti-GFP antibody and are shown in green, staining with antibodies as indicated in red, overlay in yellow and Hoechst staining in blue. Size bar 50 µm. The number of mice, replications and sample size for each experiment are shown in Supplementary Table 3.

Extended Data Figure 3 | Cre-mediated recombination induces GFP expression in myeloid or in myeloid and fibroblastoid stroma cells of MCA313$^{IFNγ-IND}$ tumours in PIG$^{Lys-Cre}$ and in PIG$^{Fsp-Cre}$ mice respectively and IFNγ signalling in T cells does not contribute to reduction in CD31$^+$/CD146$^+$ tumour endothelial cells after IFNγ induction in established tumours. a PIG$^{Lys-Cre}$ mice**, b, c** PIG$^{Fsp-Cre}$. **a** and **c,** Immunohistology. GFP signals were amplified by anti-GFP antibody and are shown in green, staining with antibodies as indicated in red, overlay in yellow and Hoechst staining in blue. Size bar 50 µm. **b**, Flowcytometry for GFP expression of primary tail fibroblasts from PIG$^{IFNγR-del}$ (n = 6) and PIG$^{Fsp-Cre}$ (n = 5) mice after 7 days of culture (mean 25.5 ± SD 12.8%). **d,** Rag^{del} (n = 6) or Rag^{del} x IFNγR^{del} mice (n = 5) were reconstituted with 2 x 10^7 splenocytes from WT mice. Two weeks after T cell transfer, MCA313$^{IFNγ-IND}$ cells were injected and IFNγ was induced when tumours were established (846 ± 263 mm^3). 5 days after IFNγ induction, endothelial cells from 10^7 tumour cells were analysed by flowcytometry. ** *P*<0.01. The number of mice, replications and sample size for each experiment are shown in Supplementary Table 3.

Extended Data Figure 4 | a, b, Tamoxifen-induced, Cre-mediated recombination in MCA313$^{IFNγ-IND}$ tumour endothelial cells of PDGFB-CreER-IRES-GFP x Rosa26-RFP mice and c-g, IFNγ-competent mice with IFNγR expression exclusively in endothelial cells show necrosis before IFNγ induction, but further reduction in blood vessel density and tumour regression after IFNγ induction. a, Tumour sections of mice, treated with tamoxifen (upper left) or not (lower left), were stained with anti-CD31 antibodies (white). RFP expression (red) indicates tamoxifen-dependent recombination, GFP signals were amplified by anti-GFP antibody and are shown in green indicating PDGFB-promoter activity, overlay in yellow, Hoechst in blue. Panels to the right show single colours of the upper left panel. Size bar 50 µm. **b,** Flowcytometry of tumour-derived endothelial cells, gated on CD31$^+$/CD146$^+$ cells, of tamoxifen-treated (right panel) or non-treated mice (left panel) reveals recombination (RFP$^+$ cells). For tamoxifen treated group, one representative out of 4 experiments is shown (mean 75.4 ± SD 8.8%) RFP$^+$ endothelial cells. **c,** In PIG$^{Pdgfb-Cre}$ mice treated with tamoxifen, GFP expression (reflecting both PDGFB-promoter-dependent Cre expression and excision of the stop cassette in PIG$^{IFNγR-del}$ mice) was detected in endothelial cells in MCA313$^{IFNγ-IND}$ tumours. **d,** MCA313$^{IFNγ-IND}$ tumours grew slower than in WT mice even without IFNγ induction and **e**, became necrotic presumably because of low-level constitutive IFNγ present in the mice and primarily IFNγR expressing endothelial cells being able to consume it. Size bar 0.5 cm **d,** IFNγ induction in established MCA313$^{IFNγ-IND}$ tumours in PIG$^{Pdgfb-Cre}$ mice induced tumour regression**,** and **f, g,** reduction of endothelial cells. **c**, GFP expression in endothelial cells of MCA313$^{IFNγ-IND}$ tumours of PIG$^{Pdgfb-Cre}$ mice. GFP signals were amplified by anti-GFP antibody and are shown in green, staining with antibodies as indicated in red, overlay in yellow and Hoechst in blue. Mice received tamoxifen starting 3 days before cancer cell injection. Size bar 50 µm. **d,** Tumour regression following dox application (dox was given at a size of 509 ± 119 mm^3; n = 5 no dox, and n = 6 with dox). **e,** Necrosis is visible in tumours before and is increased 120 h after dox-mediated IFNγ induction. **f**, Reduced blood vessel density in MCA313$^{IFNγ-IND}$ tumours of PIG$^{Pdgfb-Cre}$ mice 120 h after dox-mediated IFNγ induction. Tamoxifen treatment and immunohistology as in **c**. Size bar 100 µm. **g,** Reduced numbers of CD31$^+$/CD146$^+$ cells in MCA313$^{IFNγ-IND}$ tumours 120 h after dox application. Endothelial cells from 10^7 tumour cells were analysed by flowcytometry (n = 3 no dox, n = 4 with dox). The number of mice, replications and sample size for each experiment are shown in Supplementary Table 3.

Extended Data Figure 5 | GFP and IFNγR are expressed in MCA313$^{IFNγ\text{-}IND}$ tumour endothelial cells of PIG$^{Pdgfb\text{-}Cre\text{-}IFNγ\text{-}del}$ mice. Tumours progressing after prolonged IFNγ exposure in these mice are largely necrotic but still produce IFNγ and wound healing is impaired in PIG$^{Pdgfb\text{-}Cre\text{-}IFNγ\text{-}del}$ mice. a, GFP is expressed in MCA313$^{IFNγ\text{-}IND}$ tumour endothelial cells. GFP signals were amplified by anti-GFP antibody and are shown in green, staining with antibodies as indicated in red, overlay in yellow and Hoechst in blue. Size bar 50 µm. **b,** CD119 (1st column) and GFP expression in tumour endothelial cells from PIG$^{Pdgfb\text{-}Cre\text{-}IFNγ\text{-}del}$ mice treated (1st row, green histograms) or not treated with tamoxifen (2nd row, dotted line), PDGFB-CreER-IRES-GFP$^{IFNγR\text{-}del}$ treated with tamoxifen (3rd row, blue histograms) and PIG$^{IFNγR\text{-}del}$ treated with tamoxifen (4rd row, blue histograms) confirms that only after tamoxifen application in PIG$^{Pdgfb\text{-}Cre\text{-}IFNγ\text{-}del}$ mice both GFP and CD119 are induced. **c,** Since very few CD11b$^+$ (7.5%) and NK1.1$^+$ (4.2%) cells in the tumour stroma of PIG$^{Pdgfb\text{-}Cre\text{-}IFNγ\text{-}del}$ were GFP$^+$ (Supplementary Data Table 1b), NO production by tumour-derived CD11b$^+$ cells as read-out for IFNγ responsiveness was analysed. 4 x 10^5 purified CD11b$^+$ cells of MCA313$^{IFNγ\text{-}IND}$ tumours from mice as indicated were exposed to 250 U/ml IFNγ for 24 h, supernatants were mixed with Griess reagent and absorbance measured at 540 nm (dotted line shows detection limit) mean ± SD. **d,** H&E staining of a tumour section (from mice depicted in Fig. 2i) after around 50 days of IFNγ exposure. 1 representative of 4 mice is shown. **e,** Tumour of a mouse without dox (small central necrosis, 1 representative of 2 mice). Necrotic areas are encircled (dotted line). Size bar 2 mm. **f**, Progressing tumours still produce IFNγ. Tumours were reisolated after IFNγ induction from WT (n = 1, day 116), PIG$^{Cmv\text{-}Cre}$ (n = 3, day 92-116) and PIG$^{Pdgfb\text{-}Cre}$ (n = 3, day 65-66). Reisolated tumour cells were cultured in 500 ng/ml dox for 48 h. Supernatants were analysed by IFNγ ELISA, mean ± SD. **g, h,** Impaired wound healing in PIG$^{Pdgfb\text{-}Cre\text{-}IFNγ\text{-}del}$ mice. In the indicated mice bearing MCA313$^{IFNγ\text{-}IND}$ tumours (app. 50 mm^3), a wound of 5 mm diameter was instilled. **g,** WT (n = 3), IFNγR^{del} (n = 3) and mice with endothelial specific IFNγR expression (n = 6) were dox-treated (circles) or left untreated (squares) WT (n = 3) and IFNγR^{del} (n = 2) and mice with endothelial specific IFNγR expression (n = 4). Wound healing was recorded. Differences in mice with endothelial specific IFNγR became significant day 6 (*) and were highly significant day 18 (***). **h,** Representative pictures (WT day 14, IFNγR^{del} day 14, PIG$^{Pdgfb\text{-}Cre\text{-}IFNγ\text{-}del}$ day 21). * P<0.05, ** P<0.01 and *** P<0.001.The number of mice, replications and sample size for each experiment are shown in Supplementary Table 3.

Extended Data Figure 6 | Induction of IFNγ-GFP fusion protein induces regression of established J558L$^{IFNγ\text{-}GFP\text{-}IND}$ tumours and blood vessels. a, 10^6 J558L$^{IFNγ\text{-}GFP\text{-}IND}$ cells were injected into Rag^{del} mice that were left untreated (left panel) or treated with dox (right panel) when tumours had a size of 461 ± 230 mm^3. The crosses indicate mice that reached a humane endpoint and were taken out of the experiment (n = 10). **b,** Window chamber imaging of a J558L$^{IFNγ\text{-}GFP\text{-}IND}$ tumour at low magnification. Same procedure as described in Fig. 3c. Two weeks established J558L$^{IFNγ\text{-}GFP\text{-}IND}$ tumour was imaged for 6 days. Blue, cancer cells; green, IFNγ-GFP fusion protein and right vascular network. One representative out of 3 experiments is shown. **c** and **d,** Quantification of histological analysis for CD31 and cleaved caspase 3 (CC3) staining, respectively. Each dot represents one field of view analysed by ImageJ. **e,** Representative CD31 and CC3 staining before and 120 h after dox. **f,** Quantification of ERG$^+$ nuclei from immunohistology. **g,** Representative ERG staining before and 120 h after dox. Size bar 100 µm. Three tumours with 4-6 fields of view were analysed. *** P<0.001.The number of mice, replications and sample size for each experiment are shown in Supplementary Table 3.

Extended Data Figure 7 | Induction of TNF-GFP fusion protein induces regression of established J558L$^{TNF\text{-}GFP\text{-}IND}$ tumours and bursting of blood vessels. a, 10^6 J558L$^{TNF\text{-}GFP\text{-}IND}$ cells were injected into Rag^{del} mice that were left untreated (upper panel) or treated with dox (lower panel) when tumours had a size of 611 ± 201 mm^3. Tumours eventually relapsed due to selection of TNF-GFP loss variants (data not shown). (n = 9 no dox, and n = 10 with dox). **b,** Window chamber imaging of a J558L$^{TNF\text{-}GFP\text{-}IND}$ tumour at lower magnification. Same procedure as described in Fig. 3c. Two weeks established J558L$^{TNF\text{-}GFP\text{-}IND}$ tumour was imaged for 2 days. Blue, cancer cells; green, TNF-GFP fusion protein and right vascular network. One representative out of 4 experiments is shown. **c** and **d,** Quantification of histological analysis for CD31 and cleaved caspase 3 (CC3) staining, respectively. Each dot represents one field of view analysed by ImageJ. **e,** Representative CD31 and CC3 staining before and 120 h after dox. **f,** Quantification of ERG$^+$ nuclei from immunohistology. **g,** Representative ERG staining without and 120 h after dox. Size bar 100 µm. Three tumours with 4-6 fields of view were analysed. ** P<0.01 and *** P<0.001.The number of mice, replications and sample size for each experiment are shown in Supplementary Table 3.

Extended Data Figure 8 | Erythrocyte extravasation after induction of TNF-GFP but not IFNγ-GFP. a, J558L$^{IFNγ\text{-}GFP\text{-}IND}$ or J558L$^{TNF\text{-}GFP\text{-}IND}$ tumours were established for two weeks and mice were dox-treated for 48 h or left untreated. Then, tumour sections were stained with H&E. In the upper row light microscopy and in the lower row eosin fluorescence signals were captured. Shown are representative sections from tumours treated with dox for 48 h. Size bar = 100 µm. **b**, Quantification of erythrocytes in high magnification fields (HMF) using the ImageJ program. Number of analysed HMF: no dox IFNγ-GFP: 69 HMF, 3 tumours; 48 h IFNγ-GFP: 97 HMF, 4 tumours; no dox TNF-GFP: 130 HMF, 3 tumours; 48 h TNF-GFP: 92 HMF, 4 tumours. Groups were compared by unpaired t test. *** P<0.001.The number of mice, replications and sample size for each experiment are shown in Supplementary Table 3.

Extended Data Figure 9 | Activated blood vessels but not normal vessels regress upon IFNγ exposure and regression is accelerated in Irf4^{del} mice. IFNγ derived from T cells induces similar changes in gene expression as IFNγ from J558L$^{IFNγ\text{-}GFP\text{-}IND}$ or MCA313$^{IFNγ\text{-}IND}$ cells. a, No changes in blood vessel density in spleen and kidney after IFNγ induction. Anti-CD31 staining of kidney and spleen sections after IFNγ induction in MCA313$^{IFNγ\text{-}IND}$ tumours grown in WT mice (n = 2). Size bars 50 µm. **b,** Results of gene expression analysis as number of IFNγ-induced genes (log 2 fold change) in tumour endothelial cells of J558L$^{IFNγ\text{-}GFP\text{-}IND}$ tumours (n = 3), and kidney endothelial cells (n = 3). After IFNγ induction, there are more genes differentially regulated in kidney than in tumour endothelial cells. **c**, Venn-diagram showing the overlap between significantly differentially expressed genes (adj. P-value < 0.05) in endothelial cells of J558L$^{IFNγ\text{-}GFP\text{-}IND}$, MCA313$^{IFNγ\text{-}IND}$ tumours (dox-treated vs. untreated) and 16.113 tumours after treatment with IFNγ^{del} versus WT TCR-I T cells. **d,** Scatter plots of data from venn-diagram displaying changes of all genes presented (i.e. genes significantly deregulated in any of 3 comparisons). Endothelial cells from all three tumour types revealed strong similarity in regulated genes (Pearson correlation coefficients are calculated using all 410 genes). The union of 410 genes that were significantly differentially regulated in any of the three comparisons showed a correlation of approximately 0.8 across all 3 groups. Colours of dots match the colours of the numbers in the venn-diagram. The overlapping 10 genes (red dots) are highly deregulated in all three comparisons. **e**, Representative images of untreated or IFNγ-treated (10 ng/ml for 96 h) HUVECs, stained with phalloidin (green) and antibody against VE-cadherin (red). **f,** IRF4 is induced in mouse endothelial (SEND.1) cells 48 h after IFNγ (5 U/ml) treatment. Cells were stained with anti-IRF4 mAb, using transcription factor

staining kit, and analysed by flowcytometry (grey: isotype control, dotted line: without IFNγ, black line: IFNγ). **g,** Endothelial cells from 10^7 MCA313$^{IFNγ\text{-}IND}$ cells grown in heterozygous Irf4$^{wt/del}$ or Irf4^{del} mice that were treated with dox or left untreated. CD31$^+$/CD146$^+$ cells were analysed by flowcytometry. **h, i, j,** Immunohistology of MCA313$^{IFNγ\text{-}IND}$ tumours grown in heterozygous irf4$^{wt/del}$ or IRF4^{del} mice, either treated or not with dox and stained for **h,** ERG, **i,j,** CD31 and cleaved caspase 3 (CC3). * P<0.05, ** P<0.01 and *** P<0.001. The number of mice, replications and sample size for each experiment are shown in Supplementary Table 3.

Extended Data Figure 10 | IFNγ-mediated blood vessel regression in MCA313$^{IFNγ\text{-}IND}$ tumours of PIG$^{Pdgfb\text{-}Cre\text{-}IFNγ\text{-}del}$ mice. **a-c,** Non-apoptotic vessel regression in MCA313$^{IFNγ\text{-}IND}$ tumours. **a,** Representative staining for ERG and cleaved caspase (CC3). Size bar 100 µm. **b**, ERG$^+$ nuclei and **c** ERG$^+$/ CC3$^+$ cells. Quantification of histological analysis for **d,** CD31, **f,** CC3. **e,** Representative staining of CD31 and CC3**. g,** Quantification of histological analysis for collagen 4. **h,** Representative staining of CD31 and collagen 4 staining at 48 h at higher magnification. **i,** Representative staining of CD31 and collagen 4. White arrows in **h** and **i** indicate collagen 4 staining not associated with CD31 staining. Size bar 100 µm. **j,** Quantification of histological analysis for NG2. **k,** Representative staining of CD31 and NG2. In **d ,f, g** and **j** each dot shows one field of view analysed by ImageJ. **l,** Ratio of co-localization of NG2 and CD31. **m,** VE-cadherin, CD31 and Dapi staining without and 24 h after IFNγ induction. **n**, Electron microscopy analysis of blood vessels from MCA313$^{IFNγ\text{-}IND}$ tumours grown in PIG$^{Pdgfb\text{-}Cre\text{-}IFNγ\text{-}del}$ mice. Electron micrographs show (left) non-occluded vessel and (right) occluded vessel. Lumen of capillaries (asterisks), erythrocytes (Er), endothelial cells (En) and macrophages (M) are labelled. Size bar 5 microns. **o,** Three tumours (for each two specimen) and in total 32 vessels without dox and 38 vessels after 48 h after dox were analysed by electron microscopy for vessel occlusion (bar diagram). ** P<0.01 and *** P<0.001. The number of mice, replications and sample size for each experiment are shown in Supplementary Table 3.

Figure 1

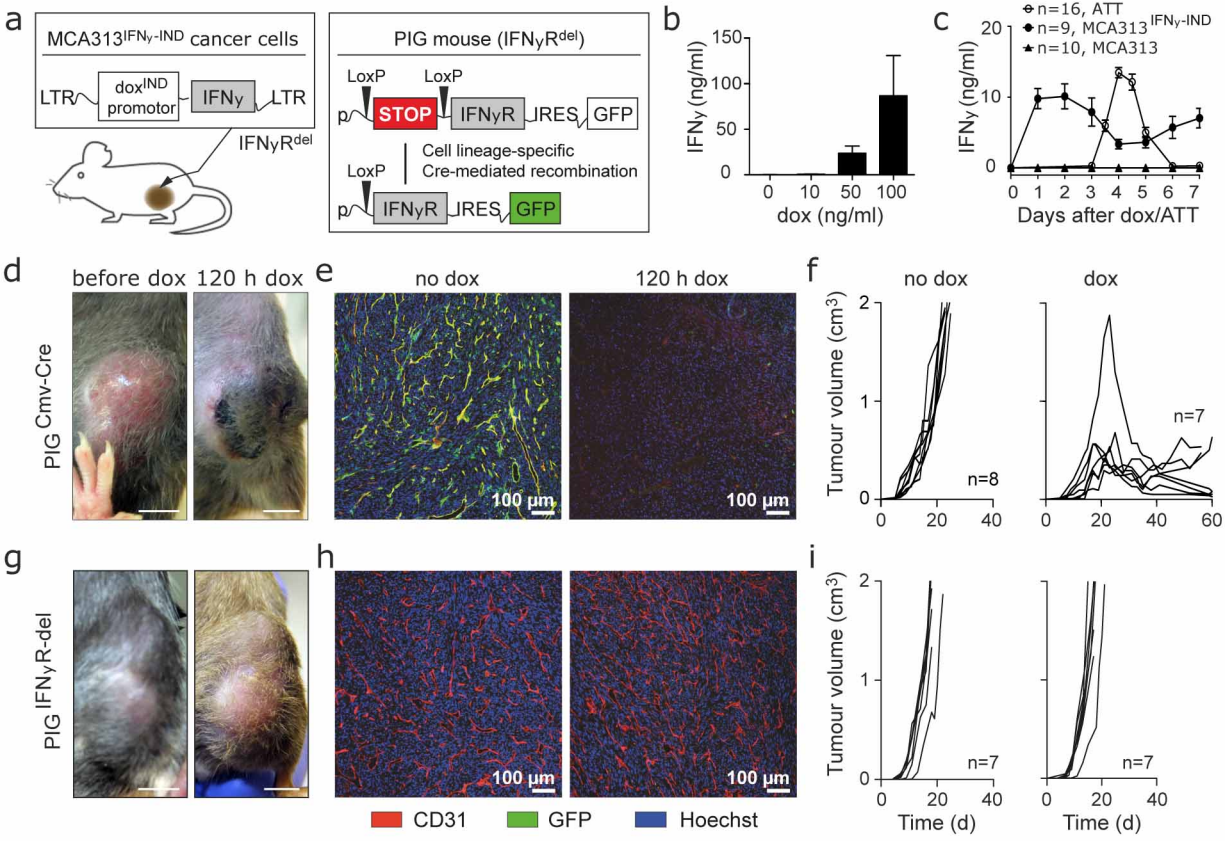
a
MCA313IFNγ-IND cancer cells
LTR
doxIND promotor
IFNγ
LTR
IFNγRdel
PIG mouse (IFNγRdel)
LoxP
LoxP
p
STOP
IFNγR
IRES
GFP
Cell lineage-specific
Cre-mediated recombination
LoxP
p
IFNγR
IRES
GFP
b
IFNγ (ng/ml)
150
100
50
0
0 10 50 100
dox (ng/ml)
c
n=16, ATT
n=9, MCA313IFNγ-IND
n=10, MCA313
IFNγ (ng/ml)
20
10
0
0 1 2 3 4 5 6 7
Days after dox/ATT
d
before dox
120 h dox
PIG Cmv-Cre
e
no dox
120 h dox
100 µm
100 µm
f
no dox
dox
Tumour volume (cm3)
2
1
0
n=8
n=7
0 20 40
0 20 40 60
g
PIG IFNγR-del
h
100 µm
100 µm
CD31
GFP
Hoechst
i
Tumour volume (cm3)
2
1
0
n=7
n=7
0 20 40
0 20 40
Time (d)
Time (d)

Figure 2

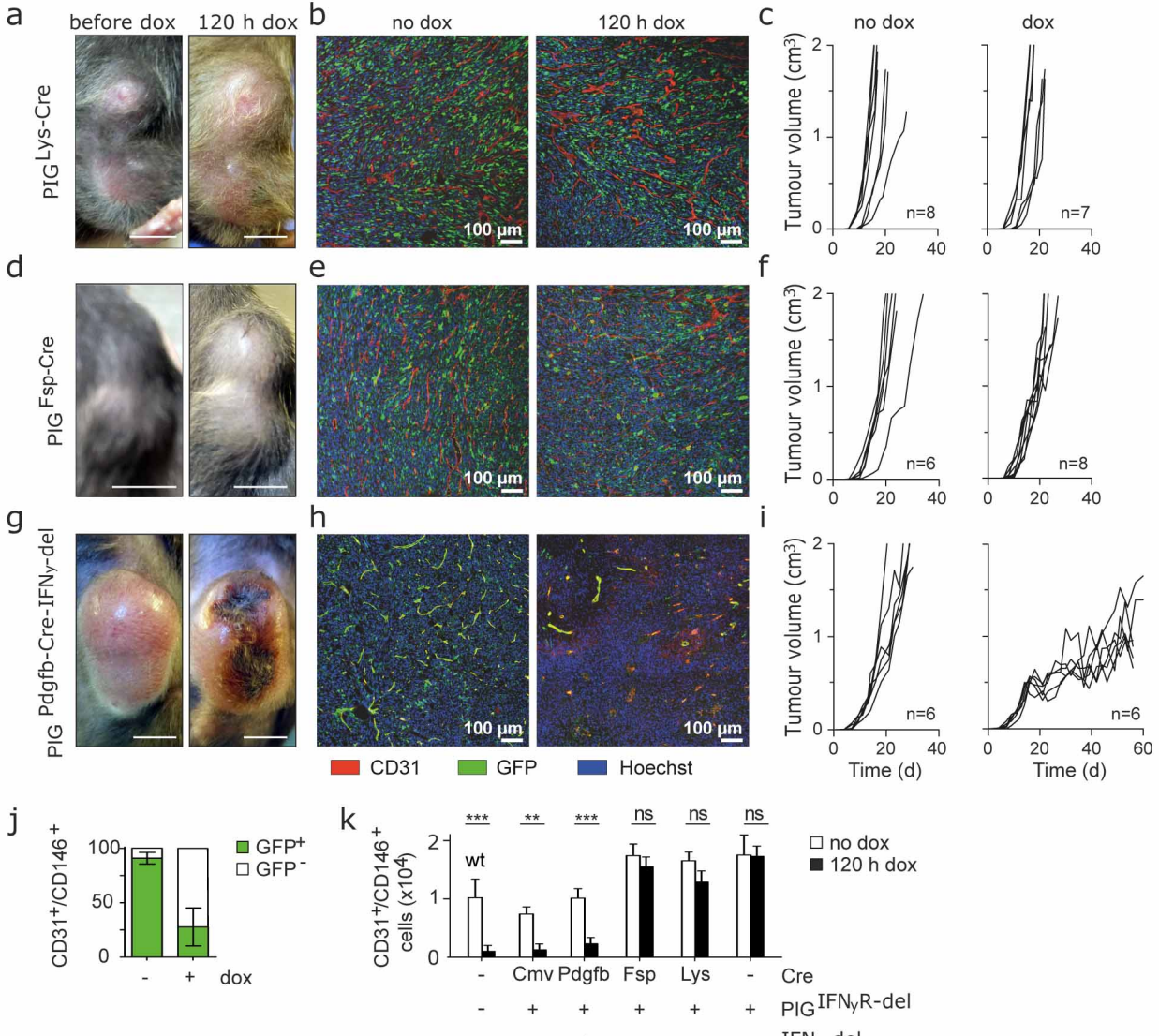
a
before dox
120 h dox
PIG Lys-Cre
b
no dox
120 h dox
100 µm
c
no dox
dox
Tumour volume (cm3)
n=8
n=7
d
PIG Fsp-Cre
e
f
n=6
n=8
g
PIG Pdgfb-Cre-IFNγ-del
h
i
n=6
n=6
Time (d)
Time (d)
CD31
GFP
Hoechst
j
CD31+/CD146+
GFP+
GFP-
dox
k
CD31+/CD146+ cells (x10^4)
wt
no dox
120 h dox
***
**
***
ns
ns
ns
Cre
Cmv
Pdgfb
Fsp
Lys
PIG IFNγR-del
IFNγ-del

Figure 3

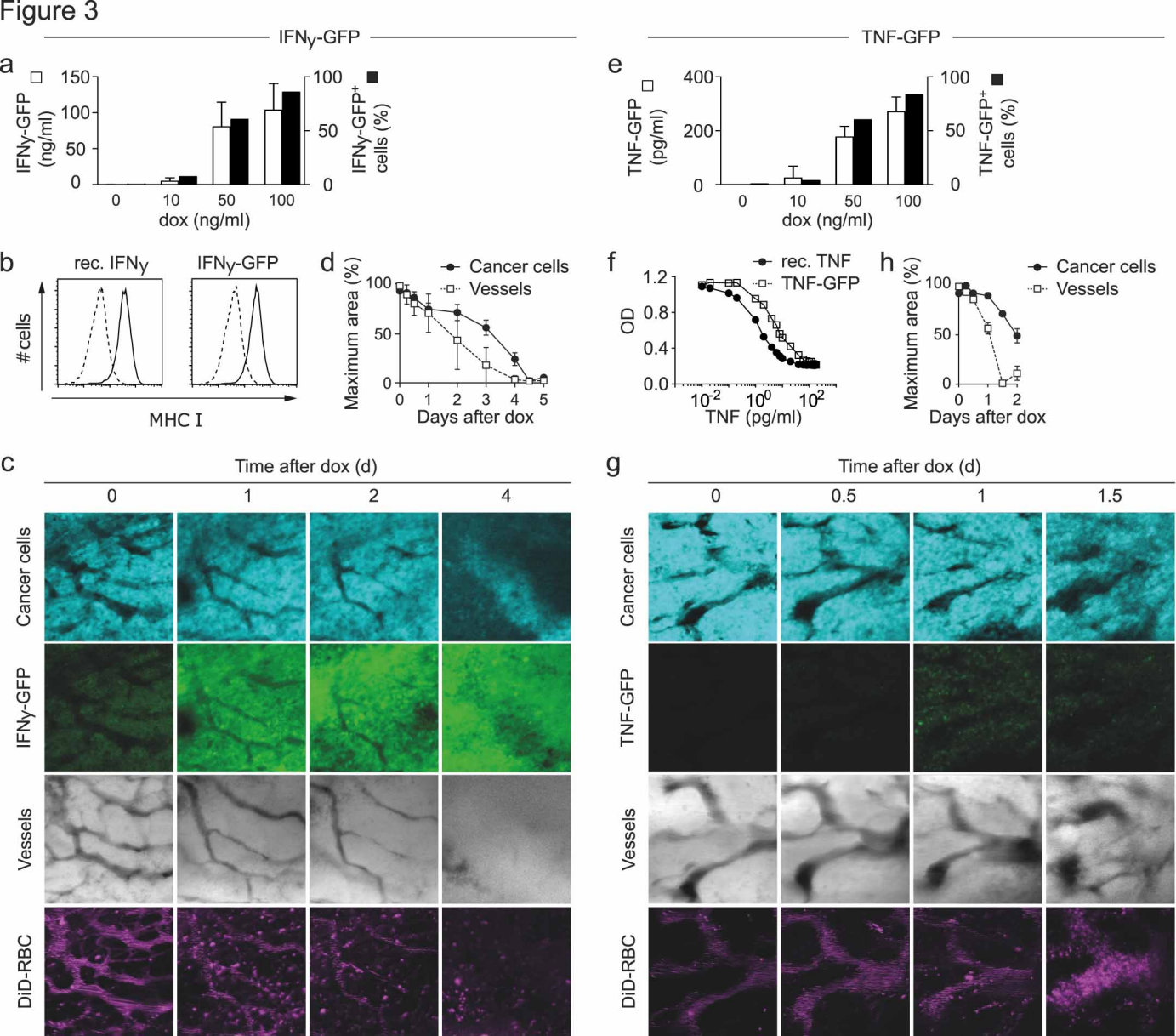
IFNγ-GFP
TNF-GFP
a
IFNγ-GFP (ng/ml)
IFNγ-GFP+ cells (%)
dox (ng/ml)
e
TNF-GFP (pg/ml)
TNF-GFP+ cells (%)
dox (ng/ml)
b
rec. IFNγ
IFNγ-GFP
#cells
MHC I
d
Cancer cells
Vessels
Maximum area (%)
Days after dox
f
rec. TNF
TNF-GFP
OD
TNF (pg/ml)
h
Cancer cells
Vessels
Maximum area (%)
Days after dox
c
Time after dox (d)
Cancer cells
IFNγ-GFP
Vessels
DiD-RBC
g
Time after dox (d)
Cancer cells
TNF-GFP
Vessels
DiD-RBC

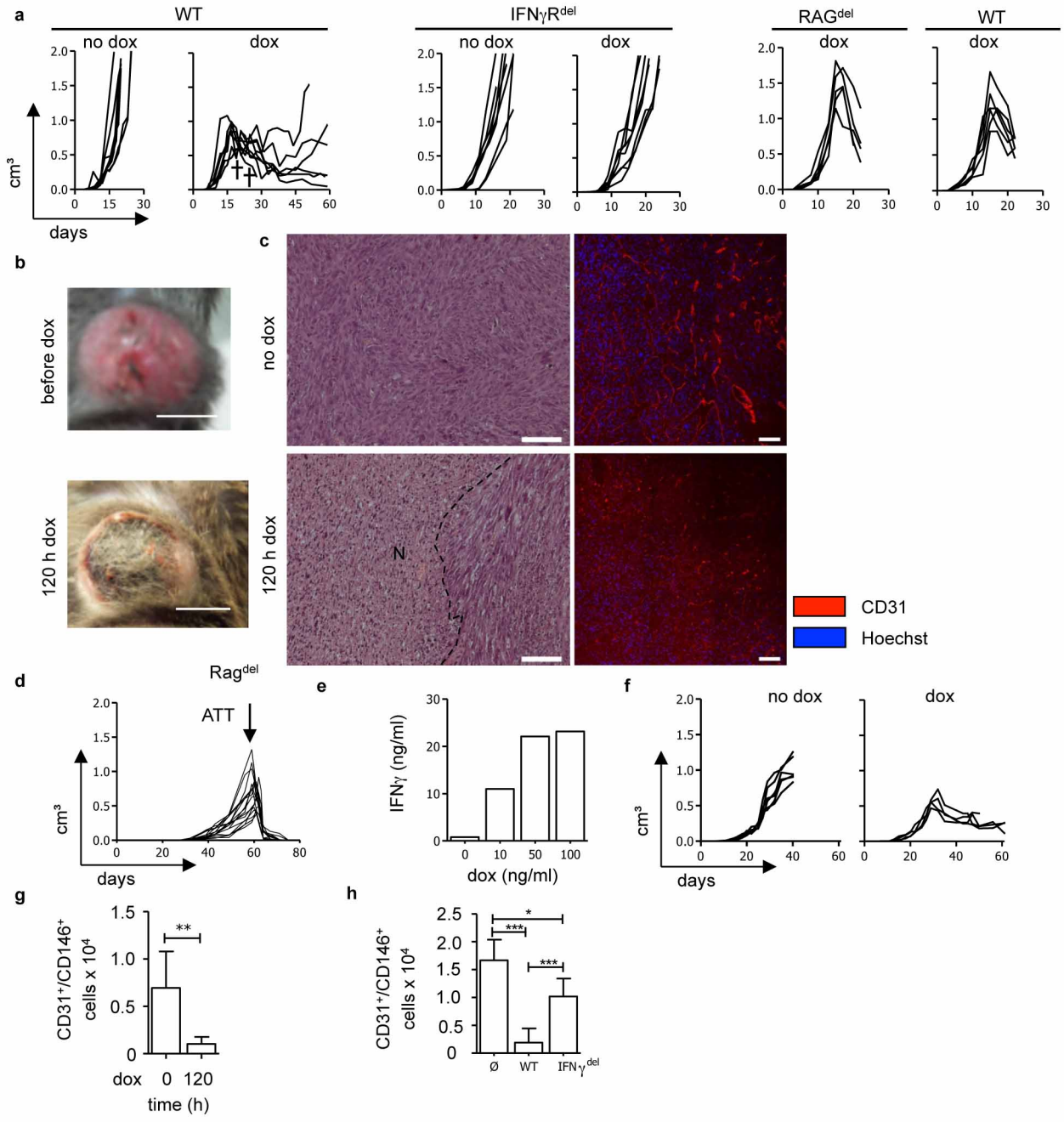
a
WT
no dox
dox
IFNγR^del
no dox
dox
RAG^del
dox
WT
dox
cm³
days
b
before dox
120 h dox
c
no dox
120 h dox
N
CD31
Hoechst
d
Rag^del
ATT
cm³
days
e
IFNγ (ng/ml)
dox (ng/ml)
f
no dox
dox
cm³
days
g
CD31⁺/CD146⁺ cells x 10⁴
**
dox 0 120
time (h)
h
CD31⁺/CD146⁺ cells x 10⁴
*
***
***
Ø
WT
IFN-γ^del

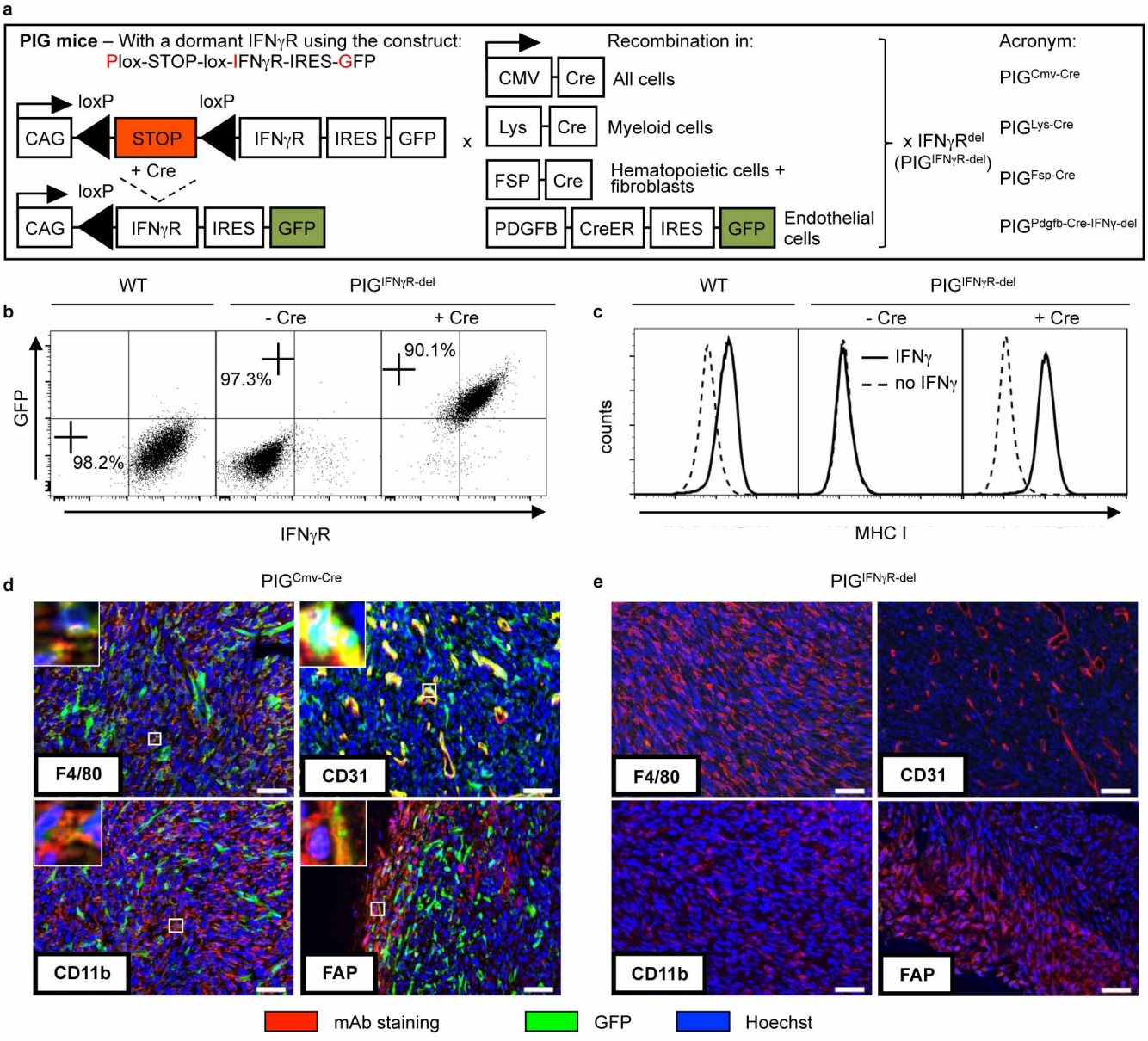
a
PIG mice – With a dormant IFNγR using the construct:
Plox-STOP-lox-IFNγR-IRES-GFP
loxP
loxP
CAG
STOP
IFNγR
IRES
GFP
x
+ Cre
loxP
CAG
IFNγR
IRES
GFP
Recombination in:
CMV
Cre
All cells
Lys
Cre
Myeloid cells
FSP
Cre
Hematopoietic cells + fibroblasts
PDGFB
CreER
IRES
GFP
Endothelial cells
x IFNγR^del (PIG^IFNγR-del)
Acronym:
PIG^Cmv-Cre
PIG^Lys-Cre
PIG^Fsp-Cre
PIG^Pdgfb-Cre-IFNγ-del
b
WT
PIG^IFNγR-del
- Cre
+ Cre
GFP
98.2%
97.3%
90.1%
IFNγR
c
WT
PIG^IFNγR-del
- Cre
+ Cre
IFNγ
no IFNγ
counts
MHC I
d
PIG^Cmv-Cre
F4/80
CD31
CD11b
FAP
e
PIG^IFNγR-del
F4/80
CD31
CD11b
FAP
mAb staining
GFP
Hoechst

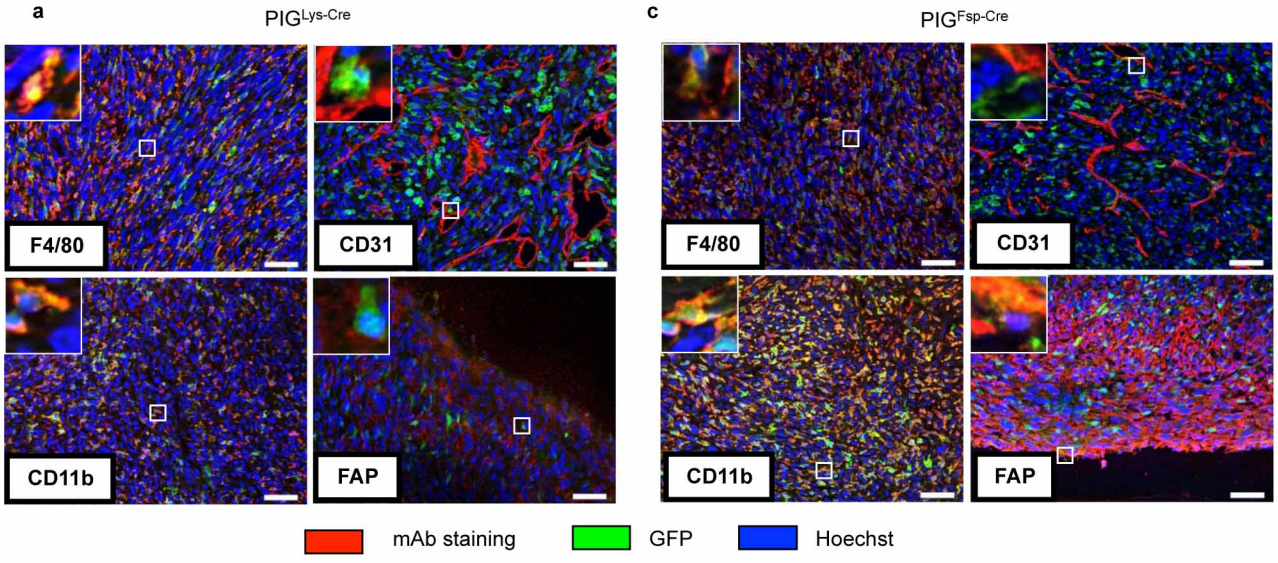
a
PIG^Lys-Cre
F4/80
CD31
CD11b
FAP
c
PIG^Fsp-Cre
F4/80
CD31
CD11b
FAP
mAb staining
GFP
Hoechst

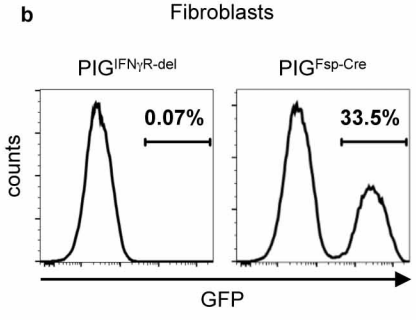
b
Fibroblasts
PIG^IFNγR-del
PIG^Fsp-Cre
0.07%
33.5%
counts
GFP

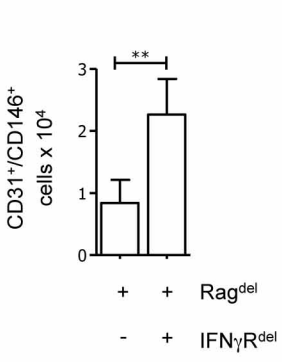
d
**
CD31+/CD146+ cells x 10^4
3
2
1
0
+ + Rag^del
- + IFNγR^del

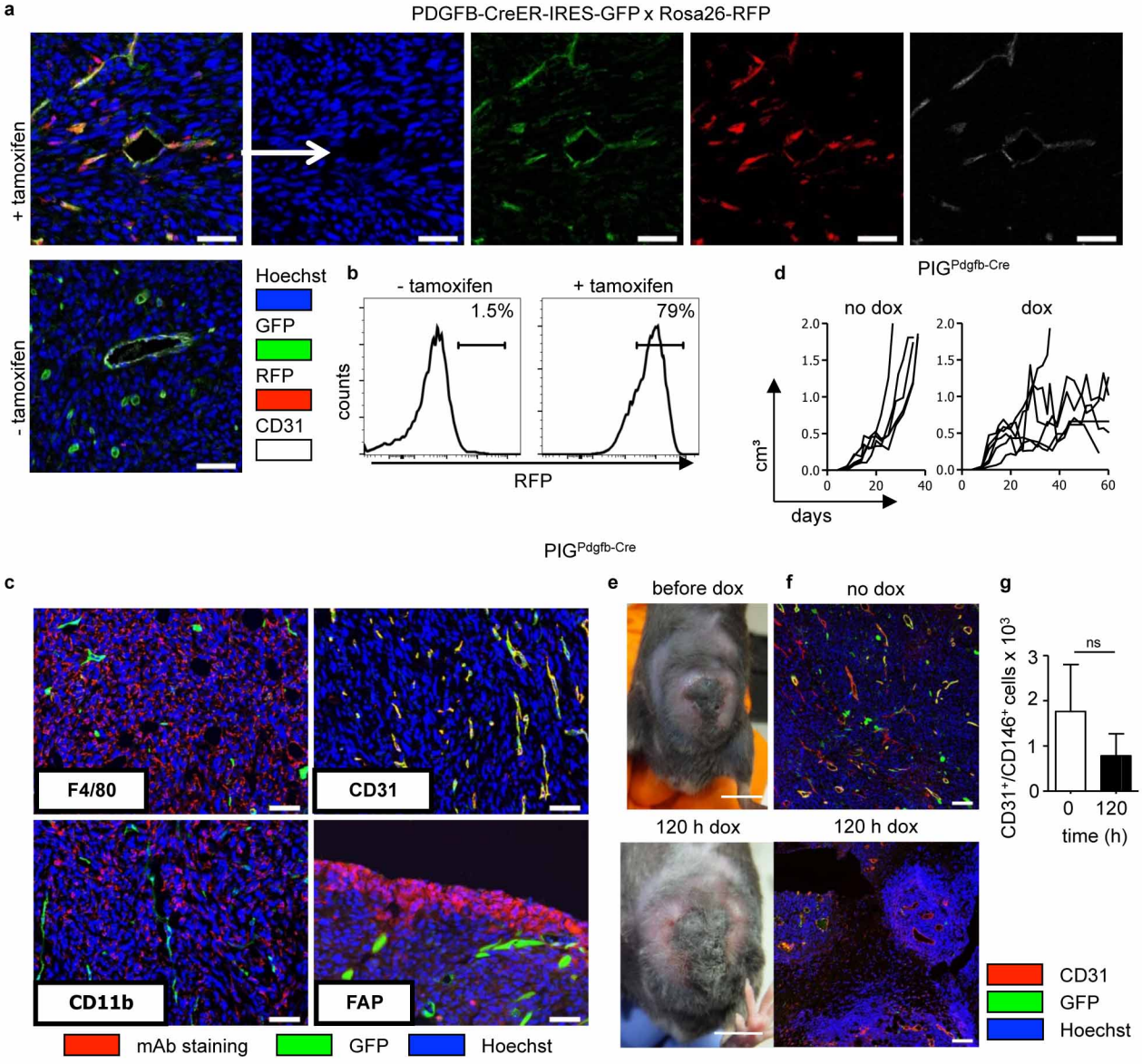
a
PDGFB-CreER-IRES-GFP x Rosa26-RFP
+ tamoxifen
- tamoxifen
Hoechst
GFP
RFP
CD31
b
- tamoxifen
+ tamoxifen
1.5%
79%
counts
RFP
d
PIG Pdgfb-Cre
no dox
dox
cm³
days
PIG Pdgfb-Cre
c
F4/80
CD31
CD11b
FAP
mAb staining
GFP
Hoechst
e
before dox
120 h dox
f
no dox
120 h dox
g
ns
CD31⁺/CD146⁺ cells x 10³
time (h)
CD31
GFP
Hoechst

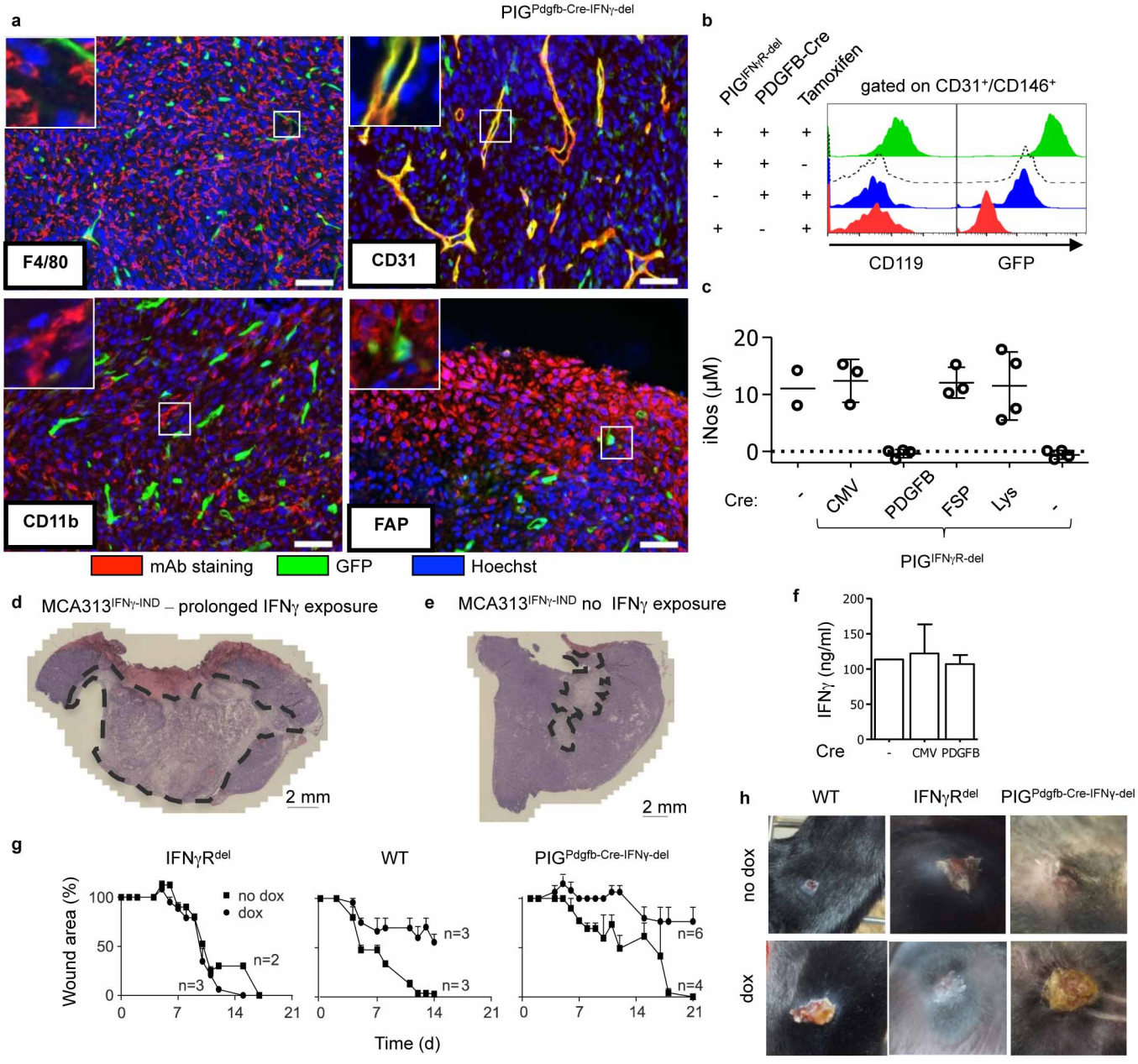
a
PIG Pdgfb-Cre-IFNγ-del
F4/80
CD31
CD11b
FAP
mAb staining
GFP
Hoechst
b
PIG IFNγR-del
PDGFB-Cre
Tamoxifen
gated on CD31+/CD146+
CD119
GFP
c
iNos (μM)
20
10
0
Cre:
-
CMV
PDGFB
FSP
Lys
-
PIG IFNγR-del
d
MCA313 IFNγ-IND – prolonged IFNγ exposure
2 mm
e
MCA313 IFNγ-IND no IFNγ exposure
2 mm
f
IFNγ (ng/ml)
200
150
100
50
0
Cre
-
CMV
PDGFB
g
IFNγR del
WT
PIG Pdgfb-Cre-IFNγ-del
Wound area (%)
100
50
0
no dox
dox
n=2
n=3
n=3
n=3
n=6
n=4
0
7
14
21
Time (d)
h
WT
IFNγR del
PIG Pdgfb-Cre-IFNγ-del
no dox
dox

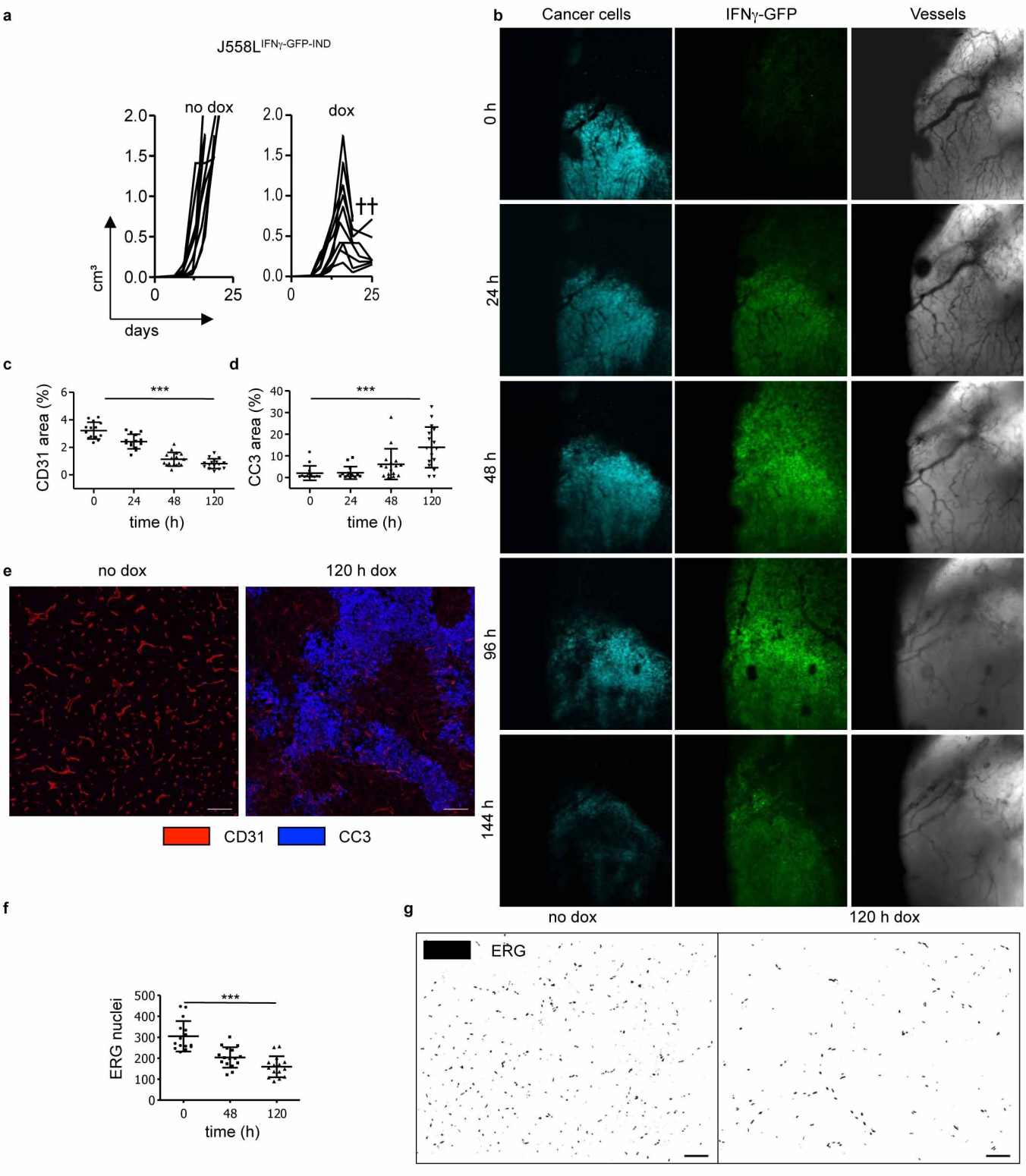
a
J558L IFNγ-GFP-IND
no dox
dox
2.0
1.5
1.0
0.5
0.0
0
25
cm³
days
††
b
Cancer cells
IFNγ-GFP
Vessels
0 h
24 h
48 h
96 h
144 h
c
CD31 area (%)
***
0
24
48
120
time (h)
d
CC3 area (%)
***
time (h)
e
no dox
120 h dox
CD31
CC3
f
ERG nuclei
***
time (h)
g
no dox
120 h dox
ERG

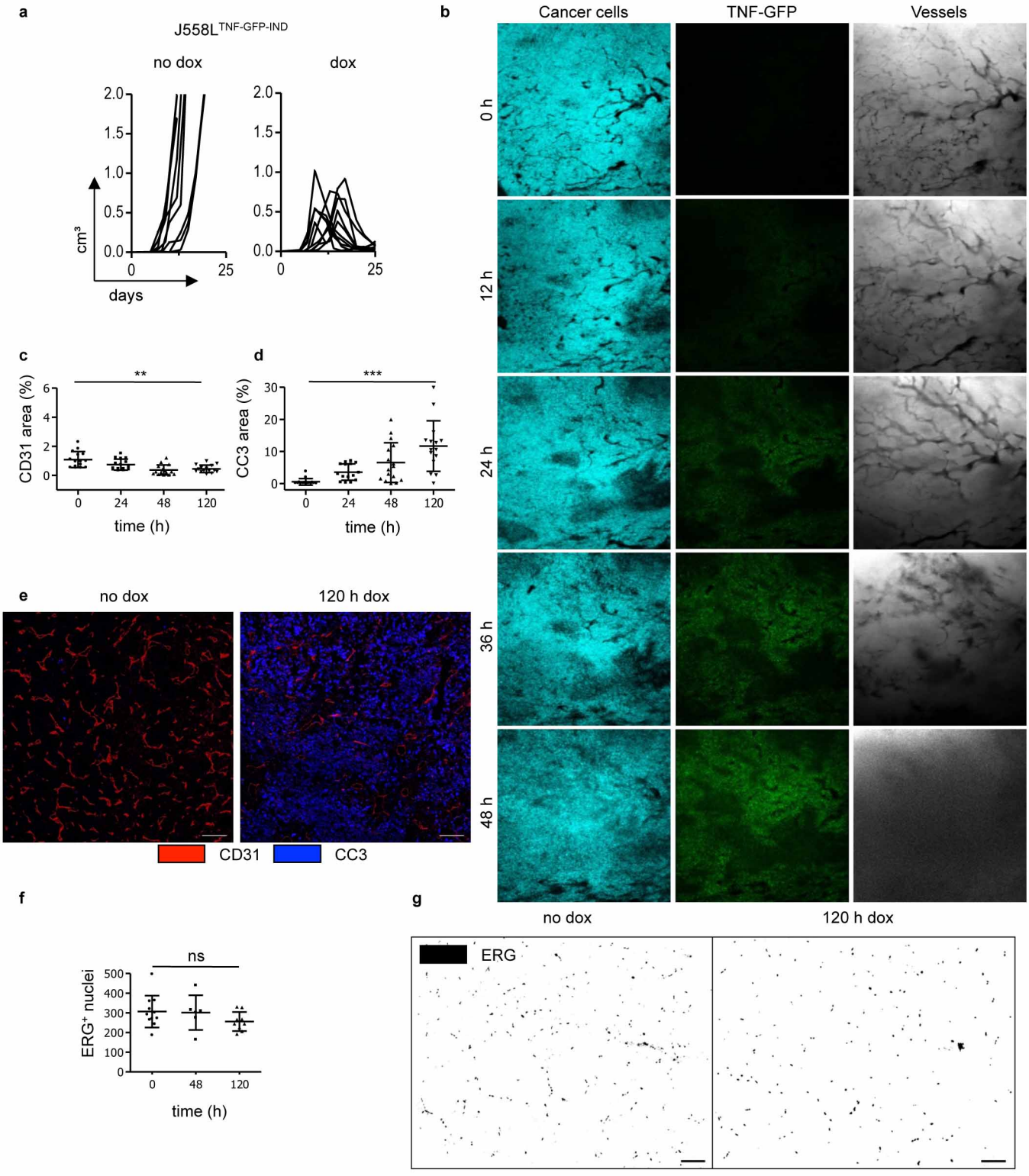
a
J558L TNF-GFP-IND
no dox
dox
cm³
days
b
Cancer cells
TNF-GFP
Vessels
0 h
12 h
24 h
36 h
48 h
c
CD31 area (%)
time (h)
d
CC3 area (%)
time (h)
e
no dox
120 h dox
CD31
CC3
f
ERG⁺ nuclei
ns
time (h)
g
no dox
120 h dox
ERG

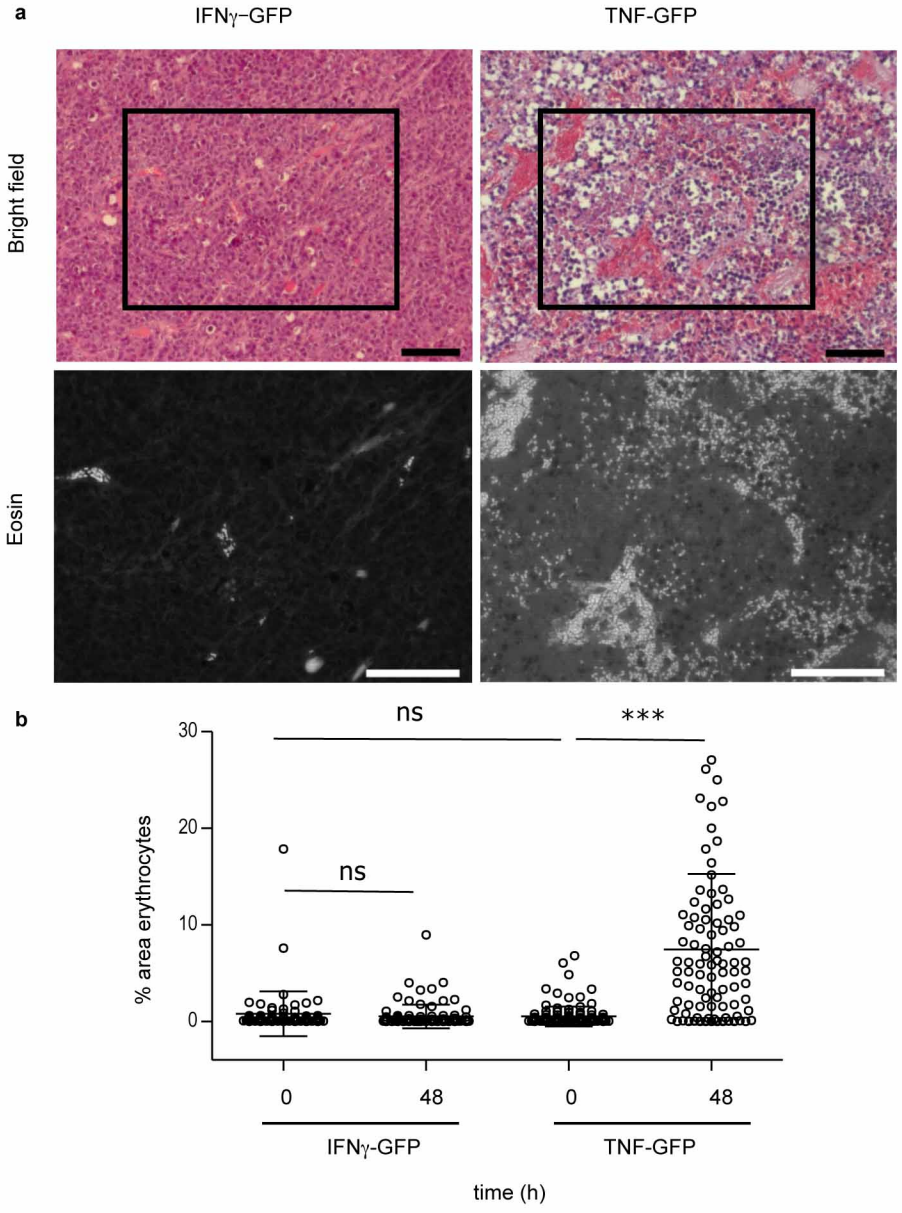
a
IFNγ–GFP
TNF-GFP
Bright field
Eosin
b
ns
***
ns
30
20
10
0
% area erythrocytes
0
48
0
48
IFNγ-GFP
TNF-GFP
time (h)

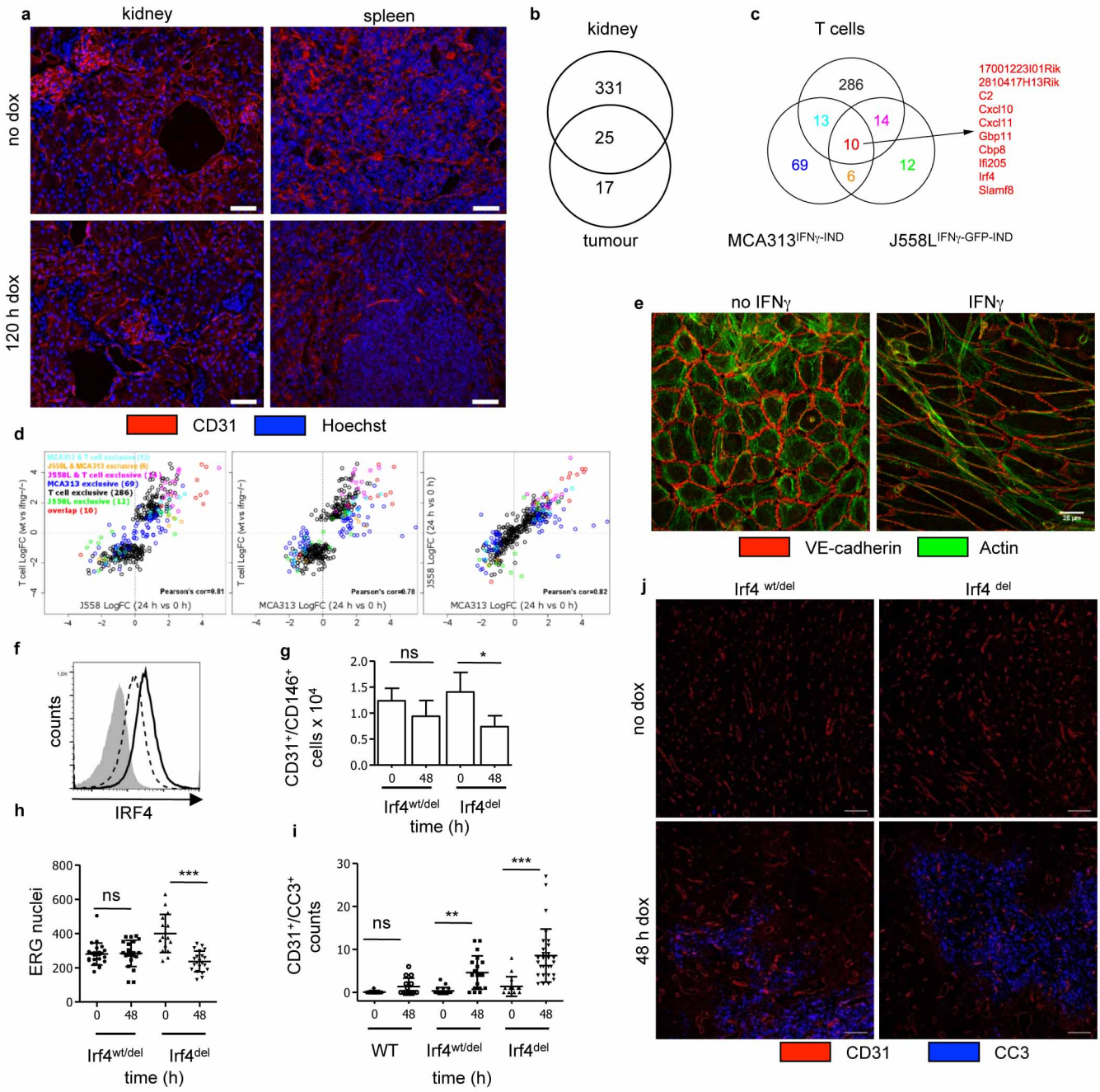
a
kidney
spleen
no dox
120 h dox
CD31
Hoechst
b
kidney
331
25
17
tumour
c
T cells
286
13
14
10
69
6
12
17001223l01Rik
2810417H13Rik
C2
Cxcl10
Cxcl11
Gbp11
Cbp8
Ifi205
Irf4
Slamf8
MCA313IFNγ-IND
J558LIFNγ-GFP-IND
d
J558 LogFC (24 h vs 0 h)
MCA313 LogFC (24 h vs 0 h)
Pearson's cor=0.81
Pearson's cor=0.78
Pearson's cor=0.82
e
no IFNγ
IFNγ
VE-cadherin
Actin
f
counts
IRF4
g
CD31+/CD146+ cells x 10^4
ns
*
Irf4wt/del
Irf4del
time (h)
h
ERG nuclei
ns
***
Irf4wt/del
Irf4del
time (h)
i
CD31+/CC3+ counts
ns
**
***
WT
Irf4wt/del
Irf4del
time (h)
j
Irf4 wt/del
Irf4 del
no dox
48 h dox
CD31
CC3

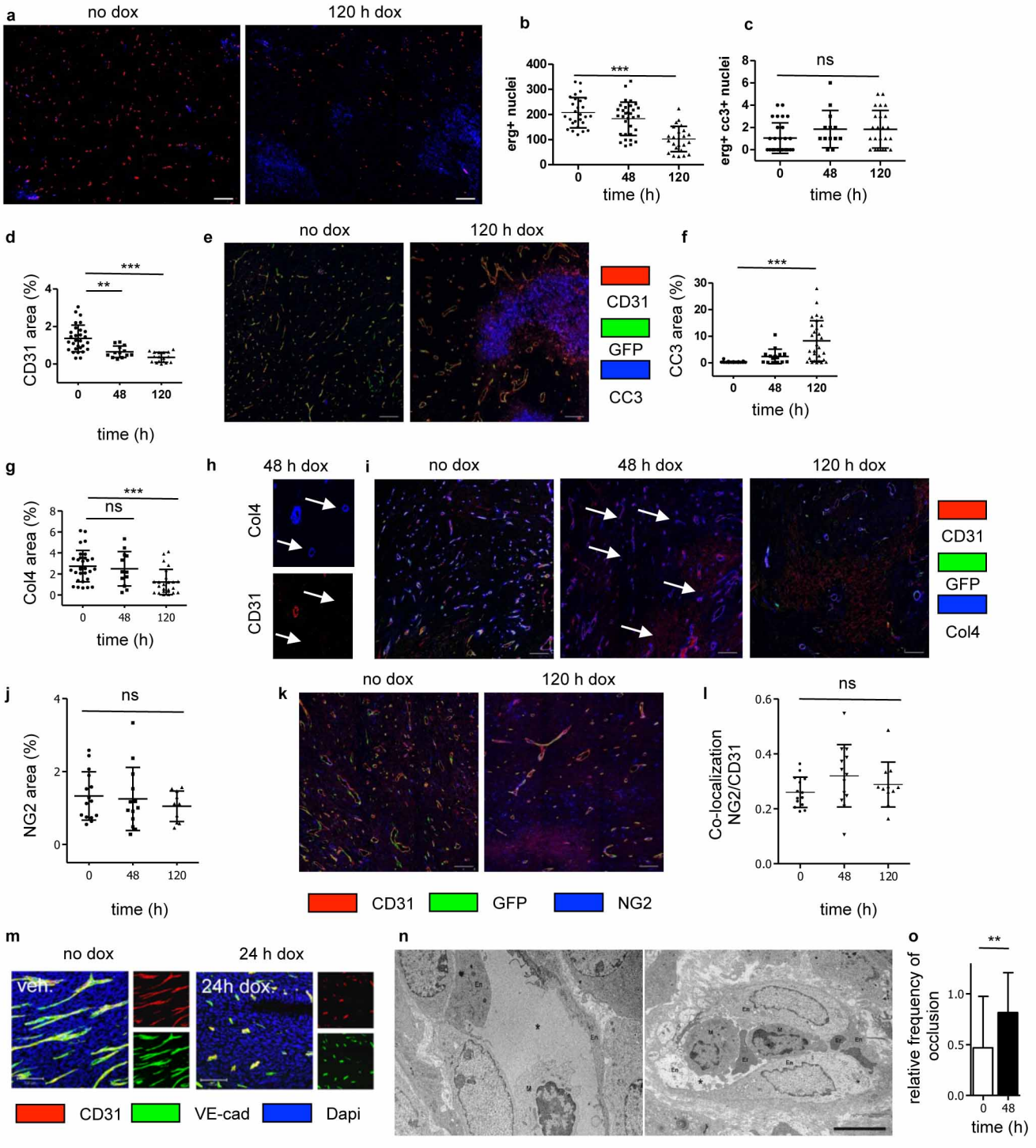
a
no dox
120 h dox
b
erg+ nuclei
***
time (h)
c
erg+ cc3+ nuclei
ns
time (h)
d
CD31 area (%)
***
**
time (h)
e
no dox
120 h dox
CD31
GFP
CC3
f
CC3 area (%)
***
time (h)
g
Col4 area (%)
***
ns
time (h)
h
48 h dox
Col4
CD31
i
no dox
48 h dox
120 h dox
CD31
GFP
Col4
j
NG2 area (%)
ns
time (h)
k
no dox
120 h dox
CD31
GFP
NG2
l
Co-localization NG2/CD31
ns
time (h)
m
no dox
24 h dox
veh.
24h dox
CD31
VE-cad
Dapi
n
En
M
Ep
*
o
relative frequency of occlusion
**
time (h)